International Journal of Heat and Fluid Flow 88 (2021) 108754

Contents lists available at ScienceDirect

International Journal of Heat and Fluid Flow

journal homepage: www.elsevier.com/locate/ijhff

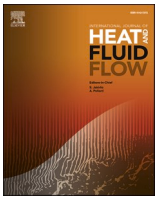

Two-phase co-current flow simulations using periodic boundary conditions in horizontal, 4, 10 and 90° inclined eccentric annulus, flow prediction using a modified interFoam solver and comparison with experimental results

C. Friedemann [a,*], M. Mortensen [a], J. Nossen [b]

[a] Department of Mathematics, University of Oslo, Moltke Moes vei 35, 0851 Oslo, Norway
[b] Institute for Energy Technology, 2007 Kjeller, Norway

ARTICLE INFO

Keywords:
Annulus
Slug flow
Wavy flow
Churn Flow
Volume of fluid
Reynolds-averaged Navier–Stokes equations

ABSTRACT

Two-phase oil and gas flow were simulated in an entirely eccentric annulus and compared with experimental data at horizontal, 4, 10, and 90° inclination. The gas-phase was sulphur hexafluoride and the liquid phase a mixture of Exxsol D60 and Marcol 82 for the inclined cases (5–16), and pure Exxsol D60 for the horizontal cases (1–4). The diameter of the outer and inner cylinders was 0.1 and 0.04 m, respectively, for the inclined domains and 0.1 and 0.05 m for the horizontal domain. The cases studied consist of liquid phase fractions between 0.3 and 0.65 and mixture velocities from 1.2 to 4.25 m/s. The mean pressure gradient is within 33% of the expected experimental behavior for all inclined cases. In contrast, the low-velocity horizontal domains exhibit significant deviation, with a drastic over-prediction of the mean pressure gradient by as much as 200–335% for cases 1 and 2. The two remaining horizontal cases (3 and 4) are within 22% of the expected mean pressure gradient. Cases 13–16 are a replication of cases 5–8 at an increased inclination; the mean pressure gradient is within 6.5% of the expected increase due to the increase in hydrostatic pressure. By comparing cases 1–4 to previous published simulations at a lower eccentricity, we found a decrease of the mean pressure gradient by 30–40%, which is in line with existing literature, although for single-phase flows. The simulated and experimental liquid holdup profiles are in good agreement when comparing the fractional data; wave and slug frequencies match to within 0.5 Hz; however, at closer inspection, it is apparent that there is a decrease in the amount of phase-mixing of the simulations compared to the experiments. When increasing the mesh density from 115 k cells/m to 2 million cells/m, the simulations exhibit significantly more phase mixing, but are still unable to produce conventional slugs. In a simplified case, conventional slugs are observed at grid sizing of $1 \times 1 \times 1$ mm, whereas the cells of the 2 million cells/m mesh are roughly $1.5 \times 1.5 \times 1.5$ mm.

1. Introduction

The study of two-phase flow through simulations is a complex and time-consuming exercise, yet important in order to complement the existing experimental literature. It is crucial to understand multiphase flow within an annulus, because of its purpose and prevalence in industry. In the petroleum industry, annuli are found within wells and pipe-in-pipe heating systems in pipelines and risers and transients, pressure gradient and flow regime prediction are imperative for flow assurance, pipeline maintenance and design. In the nuclear industry, similar geometries are found related to the cooling rods, and it is even found in the aerospace industry within the combustion chamber of an engine. These industries share the potential for catastrophic failures to occur, which will impact the environment and ecosystem, and potentially prove fatal.

Simulations allow us to gaze into the behavior of flow within complicated geometries. Several facets make the annulus geometry studied in this work a complex problem, such as the size and relative positions of the two cylinders. In addition, the annulus configuration represents a simplified version of more complex geometries, including rod bundles in a nuclear reactor (Julia and Hibiki, 2011). Fluid interaction with the interior cylinder also causes the friction factor to be a

* Corresponding author.
E-mail address: chrisjfr@student.matnat.uio.no (C. Friedemann).

https://doi.org/10.1016/j.ijheatfluidflow.2020.108754
Received 10 April 2020; Received in revised form 14 September 2020; Accepted 12 November 2020
Available online 18 January 2021

function of the annulus eccentricity.

One of the factors studied in this work is the effect of eccentricity, while all present cases are fully eccentric, the effect is studied based on previous published work (Friedemann et al., 2020). Eccentricity is a measure of the relative positions of the cylinder centers. The annulus is fully eccentric when the distance between the two cylinder centers is maximized, while the annulus is concentric when the centers coincide. Although it is easily assumed that the friction factor is increased due to the surface area introduced through the inner cylinder, multiple sources state that for an eccentric annulus, the friction factor is always lower than for an equivalent hollow pipe, and the opposite for a concentric annulus (Denton, 1963; Caetano, 1985). In addition, the rate of change of the friction factor is not linear and depends on whether the flow is turbulent or laminar (Hanks and Bonner, 1971). We must also consider the variable interface as the liquid height varies with the flow regime leaving a thin liquid lubricating film on the cylinder. For periodic flow, such as slugs or waves, the cross-sectional holdup oscillates, thereby creating a variable phase-interaction with the cylinder walls.

The annulus configuration has been studied experimentally since the early 1960s, when Denton (1963) wrote his thesis on turbulent flow in a concentric annulus and Vaughn (1963) studied laminar flow of non-Newtonian fluids. However, these studies were based on single-phase flows; two-phase flow models were developed at a significantly later time.

The modern-day study of two-phase annulus flow was initiated by Kelessidis and Dukler (1989) and Kelessidis and Dukler (1990), who published several papers on vertical gas–liquid flow, discussing flow regime transition point modeling. Their work could be seen as an extension of the correlation-based modeling for horizontal (Taitel and Dukler, 1976) and vertical (Taitel et al., 1980) tubing. Although correlations are a historically significant part of multiphase-flow studies, they have one crucial flaw; they are by nature extremely application sensitive. Factors that may interfere with a correlation model's accuracy are fluid properties, annulus dimensions, flow rates and holdup fractions, as mentioned by Julia and Hibiki (2011), and shown by Ozar et al. (2008) in their work related to modeling of transition points of two-phase flow in an annulus. Beyond transition point modeling and flow regime mapping, studies have explored pressure losses (Erge et al., 2015; Ozbayoglu and Sorgun, 2010), pressure gradients (Ferroudji et al., 2019; Ibarra and Nossen, 2019), void fractions (Harvel et al., 1999), heat transfer (Hamad et al., 1998), slug frequencies, and Taylor bubble rise velocity (Das et al., 1998; Hills and Chéty, 1998).

Although there are recent computational studies, such as the research by Kiran et al. (2020) using Fluent to study annular flow in a vertical annulus and the work by Friedemann et al. (2019) and Friedemann et al. (2020) analyzing pressure gradients and slug frequencies in concentric and partly eccentric annuli, the vast majority of multiphase studies are experimental. However, there are several published articles that focus on other aspects of computational annulus flow including those analyzing buoyancy induced flows (Iyer and Vafai, 1998), turbulent flow and heat transfer (Nikitin et al., 2009), and natural convection (Adachi et al., 2007; Mizushima et al., 2001; Yoo, 2003; Yu et al., 2005).

Before simulations can be considered as predictive of behavior within a flow conduit, it is essential to verify simulations with experiments. The authors have previously worked on horizontal simulations in a concentric annulus configuration (Friedemann et al., 2019) and shown that the simulations are accurate within 25% of the expected pressure gradient and within 10% of the expected slug frequency. However, some simulation artifacts are hard to minimize; for example that conventional slugs are replaced by proto-slugs. A proto-slug is a structure that behaves as a slug but falls short of fulfilling conventional slug criteria. Mainly, it is observed that the proto-slug seldom covers the cross-section. It is possible that the proto-slugs stem from a lack of mesh resolution and thereby an inability to resolve minor bubbles immersed within the liquid. In simplified slices conventional slugs occur when the mesh elements are 1x1x1 mm. For coarse meshes, large gas bubbles accumulate toward the top of the annulus as their rise velocities are higher and thus they are more likely to overcome the turbulent dispersion as compared to smaller bubbles. In a typical slug, small gas bubbles permeate through the liquid, which we observe in the simplified slices; however, there are other possible explanations such as surface tension, wall effects, and choice of boundary conditions.

Pressure gradient transients are essential for industrial applications because it affects the operating limits, maintenance schedule, cost, and impact of potential ruptures. Flow regime and slug frequencies are also crucial; with this information, preventive steps can be taken to minimize slugging using slug catchers (gas/liquid pre-separators that can accommodate large slugs) and establish accurate leakage estimates in the case of a malfunction using slug frequency and holdup fractions as estimation parameters.

Finally, there is inclination, which is an essential parameter to study due to its effect on flow regime and pressure drop (Wongwises et al., 2006). There may be various solutions for transport in specific petroleum fields; some pipelines extend along the seabed, while others run vertically up to an offshore facility (Ozbayoglu et al., 2012). Different transport solutions suggest we have to account for the effect of a variable inclination. Therefore, the 10° cases are simply the 4° cases at a higher inclination, in order to study potential changes, such as backflow in the narrow region of the annulus or in the film region of a slug (Hernandez-Perez, 2008). Inclined flow is a perfect candidate for CFD studies, due to the physical restrictions imposed on an inclined experimental flow loop. In order to study inclined flow, the test section must be long for the flow to fully develop. Physical restrictions are easily overcome computationally; however, simulations come with their own limitations, mostly related to the solution time's exponential scaling tied to mesh density.

Although CFD as a tool to study multiphase flow is becoming more prevalent, extensive studies for annuli are rare. Furthermore, horizontal and vertical configurations dominate the existing literature. In this paper, a small spectrum is studied; horizontal, 4°, 10° and vertical. Ideally, steep inclinations would also be studied, but preliminary studies indicate that periodic boundary conditions and steep inclinations produce an unexpected amount of back-flow. Given the theoretical framework, the solutions are possible and highlight that periodic boundary conditions do have some problems. Studies must be careful to examine whether the behavior is representative of experimental results. The amount of liquid within the domain is determined by the initial conditions; therefore, simulating slug flow in a too short domain could result in insufficient liquid to form slugs. Similarly, if the domain length is an odd multiple of the slug to slug length, then the slug frequency could be affected.

Prohibitive solution time is another drawback. Periodic boundary conditions alleviate the computational demands by simulating an "infinite" pipe. With normal boundary conditions, in order for a slug to form, the domain needs to allow the flow to transition from a stratified inlet flow. The required domain length depends on the flow regime and phase properties. Ideally, the domain would be of the same size as the experimental loop which in our case, translates to 50 m. The fastest of our current simulations took roughly three weeks on four cores when each core was assigned 200 k cells. Axtmann et al. (2016) studied the scalability of OpenFOAM and suggests 15–20 k cells/core. We experience that the scaling reduces at around 80 k cells/m. It should be noted that Axtmann's research was done on single-phase flows, and that scaling can depend on the network configuration and communication protocols. If we extend the domain to 50 m and assume the scaling stays constant, each simulation would require 40 cores. Unfortunately, with our computational resources, that is not a viable option while covering several configurations and initial conditions.

The focus of this paper is two-phase flow within an entirely eccentric annulus. The flow behavior in four inclinations; 0, 4, 10, and 90° is studied using a modified (inclined) version of the OpenFOAM solver interFoam and regular interFoam (horizontal), in combination with periodic boundary conditions. These horizontal simulations are similar

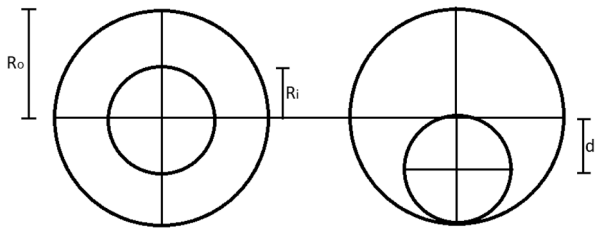

Fig. 1. Eccentricity of annulus, R_o = outer cylinder radius, R_i = inner cylinder radius, d = distance between cylinder centers.

to and share experimental data with previous simulations which were partly eccentric (E = 0.5) (Friedemann et al., 2020), with the main difference being the use of an entirely eccentric annulus. Even minor changes to the eccentricity of the annulus can have a significant effect on the flow regime, pressure gradient, and velocity profile, therefore the present simulations should be considered a novel geometry. Each simulation is accompanied by an experiment, except the 10° simulations which are a modified iteration of the 4° simulations. The experimental mixture velocity and phase fractions are used to initialize the simulations while we compare the pressure gradient, flow regime, wave or slug frequency, and the effect of a change of inclination on the above parameters.

Although CFD has come a long way since its inception, it is likely still too early to consider CFD robust and error-proof enough to replace, mechanistic models, correlations and flow regime maps for two-phase flows with petroleum applications. However, combining CFD with experimental data and comparing the results, eventually CFD can at the very least supplement the existing experimental data bases with additional metrics which are easier to evaluate through CFD and potentially be considered predictive with enough research and validation, especially for geometries that are difficult to study in a laboratory environment. This paper is a step towards prediction and validation.

2. Geometry and mesh

The geometry studied is an approximation of a fully eccentric annulus, the outer cylinder diameter is 0.1 m for all cases, while the interior cylinder diameter is 0.05 (horizontal) and 0.04 m (inclined). The domain is studied in both horizontal and inclined orientations. The inclined (and vertical) cases are at 4,10 and 90°. The eccentricity (E) of the annulus is defined a function of the radii of the inner (R_i) and outer (R_o) cylinder, as well as the distance between cylinder centers (d) as illustrated in Fig. 1 and expressed in Eq. (1)

$$E = \frac{d}{R_o - R_i}. \tag{1}$$

Eccentricity plays an essential role on flow formation by affecting the friction factor. When the distance between the cylinder centers is maximized, the annulus is fully eccentric, while an annulus where the centers coincide is fully concentric. The annulus is designed with the interior cylinder resting against the bottom wall of the outer cylinder, there is a tiny gap (0.5 mm) between two cylinders modeled as a wall, resulting in E = 0.983 and 0.98 for the inclined and horizontal domains respectively.

Meshing an eccentric annulus is complicated due to the tiny gap between the cylinders where the walls converge. Because OpenFOAM prefers hexahedral elements, in order to have the majority of elements well arranged, there are two small regions of distorted elements. The elements in question are mostly within the region where the flow velocity is decreased due to wall effects. OpenFOAM's built-in tools report no overly skewed or distorted elements, and the maximum skewness and non-orthogonality are within the OpenFOAM accepted limits of 70 for non-orthogonality and 4 for cell skewness, the maximum non-orthogonality is 65, and cell skewness is 0.68, while the average non-orthogonality is 16.

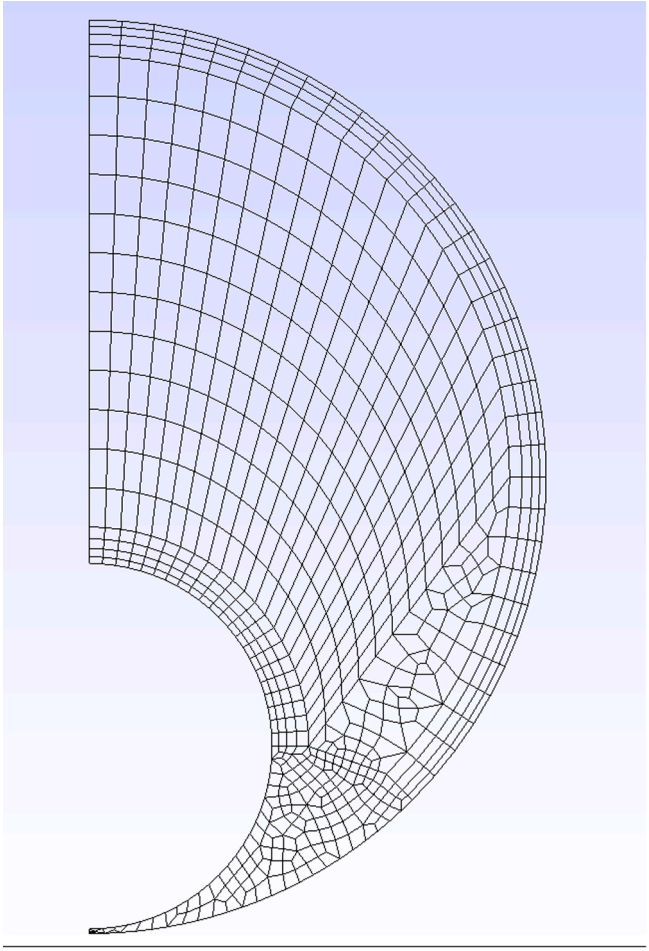

Fig. 2. Cross-sectional view of computational domain with R_0 = 5 cm and R_i = 4 cm.

The meshes employ a constant axial cell spacing of 3.9 mm, while the cross-sectional cell size vary as a function of the wall to wall distance (Fig. 2). Each mesh is approximately 115 k cells/m unless otherwise specified, and the domains utilized are 5 m in the inclined cases and 7 m for the horizontal cases. The walls are treated with wall functions, which relax the resolution requirements. The available wall functions are so called adaptive wall functions, which allows the first cell center to be located either within the log-layer or within viscous sub-layer (Kalitzin et al., 2005; Liu, 2016), some are even reportedly acceptable within the buffer layer, although steps were made to avoid this region. The viscous sublayer is located at dimensionless wall distance (y^+) below 5, and the log-layer exists for $30 \leqslant y^+ \leqslant 200$. For the 16 cases presented, the average y + is $38 \leqslant y^+ < 68$.

The initial conditions for the flow field was described using built-in OpenFOAM commands, and was based on the holdup fractions,mixture and superficial velocities attained from the experimental data (Fig. 1). For the horizontal and low inclination simulations, the flow was initialized as a stratified flow with holdup fractions and slip velocity according to the phase velocities, while the vertical simulations were initialized as intermittent sections of oil and gas. For all cases the flow is driven by a momentum-source equivalent to the experiment mixture velocity, this momentum-source is specified in the case files.

Periodic boundary conditions are applied to the domain. The entire flow field is thus transferred seamlessly through two "adjacent" patches, in this case the inlet and outlet. The flow transfer ensures that even in a short domain the flow field is allowed to developed in an "infinite" pipe. With this approach, some flows like wavy flow are almost independent

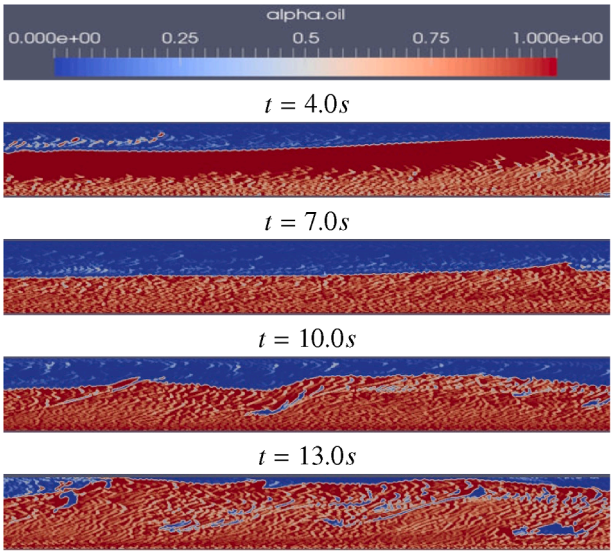

Fig. 3. Snapshots of simplified geometry inclined at 4° with gas in blue and liquid in red and cell volume = $1e-9\ m^3$.

of domain length, while other flows like slug flow could be drastically altered due to the set amount of liquid within the system (Frank, 2005; Friedemann et al., 2019). The slug frequency dependency occurs because the phase fractions are set by the initial conditions. Therefore, it is essential to pay close attention to specific parameters such as slug to slug length and phase velocities when creating a domain with the intent of utilizing periodic boundary conditions.

Vertical domains are less reliant on the domain's length as there are fewer domain length-dependent structures such as slugs. As we know, most slugs are a mixture of liquid and gas. By restricting the amount of liquid within the domain, if the domain length is not scaled to an integer value of the slug to slug length, then the slug frequency could be severely altered. The effect is minimized in domains with space for several concurrent slugs. Lastly, the low mesh density restricts bubble formation because the mesh is too coarse to resolve minor gas bubbles within the liquid layer. Instead, the gas tends to coalesce and form large bubbles which may be within the liquid layer but are typically near the top. Due to the bubble coalescence, we often observe similar holdup patterns to the experiments in terms of the cross-sectional holdup, however, the liquid does not cover the cross-section and thus does not conform to the definition of a slug. We have simulated conventional slugs in a simplified geometry without the interior pipe and a cell size of 1x1x1 mm (Fig. 3-4). The simplified case is best compared to simulation case # 6 as it has the same phase fractions, inclination, and mixture velocity.

The flow field (Fig. 3) shows the effect of phase mixing. At $t = 4.0$ s a massive wave has introduced gas into the lower liquid layer recognized by the light red patches. Ideally, in a VOF simulation, the domain should be refined until the flow is completely resolved. In a completely resolved flow, one of the visible results is that the smallest bubbles are resolved by several cells, which would reduce the large sections of cells in Fig. 3 which are neither red or blue and are represented by a mixture color. In such a refined mesh, if the contour range is reduced to 2, the phase field would be near identical to a larger contour range, because the majority of cells would be single phase, apart from the cells which contain an interface. As time progresses, the mixing increases, and gas bubbles permeate throughout the liquid, wave merging results in a naturally occurring slug at 13.0 s. Unfortunately, this mesh results in excess of 10 million cells/m if employed for our annulus, which is beyond our computational resources. As the small bubbles are introduced at very fine meshes, it is likely a grid independence test would result in a false positive. We have found the solution to be "mesh independent" in terms of pressure gradient and flow regime at around 400 k cells/m (Friedemann et al., 2019); at this stage, there are few bubbles, and the solution is near identical to both a 200 k and 500 k cells/m mesh in terms of statistical pressure and slug frequency behavior, true mesh convergence is likely reached at a much higher mesh density.

3. InterFoam and fundamental equations

InterFoam is a volume of fluid (VOF) type multiphase solver in OpenFOAM, and solves the continuity and momentum equations for an averaged fluid. One benefit of the VOF approach is that it saves computational time; however, by averaging the phases some information about phase behavior is lost. The averaging of the fluid properties is performed using conventional mixture rules based on the phase fraction within a cell. As an example, the mixture viscosity or phase-averaged viscosity is calculated as

$$\overline{\nu} = (1-\alpha)\nu_g + \alpha\nu_l. \tag{2}$$

In Eq. (2), α is the liquid fraction within a computational cell, while ν_g and ν_l are the gas and liquid viscosities. The phase fraction (α) is described as

$$\alpha = \begin{cases} 1 & \text{if cell is occupied by liquid} \\ 0 < \alpha < 1 & \text{if cell contains both gas and liquid} \\ 0 & \text{if cell is occupied by gas.} \end{cases} \tag{3}$$

α is 1 if the cell is filled with liquid, and 0 if filled with gas, and a fraction between 0 and 1 if both phases are present. The indicator function α is solved for in a modified advection equation (Eq. 4)

$$\frac{\partial\alpha}{\partial t} + \nabla\cdot\left(\alpha\overline{u}\right) + \nabla\cdot\left(u_c\alpha\left(1-\alpha\right)\right) = 0, \tag{4}$$

where the interface compression velocity, u_c, "compresses" the surface, in effect sharpening the interface. With phase-averaging implemented, and assuming incompressible flow, the governing continuity (Eq. 6) and momentum (Eq. 5) equations can be simplified as

$$\frac{\partial\overline{u}}{\partial t} + \nabla\cdot\left(\overline{u}\overline{u}\right) = -\frac{1}{\overline{\rho}}\nabla p + \nabla\cdot\left(\overline{\nu}\left(\nabla\overline{u} + (\nabla\overline{u})^T\right)\right) + g + \frac{F_s}{\overline{\rho}}, \tag{5}$$

$$\nabla\cdot\overline{u} = 0, \tag{6}$$

where $\overline{\rho}, \overline{\nu}$, and F_s represent mixture density, viscosity, and surface tension force, while $\overline{u}$ is the shared velocity field (Berberovic et al., 2009; Rusche, 2002). The calculation of the mixture components follows the

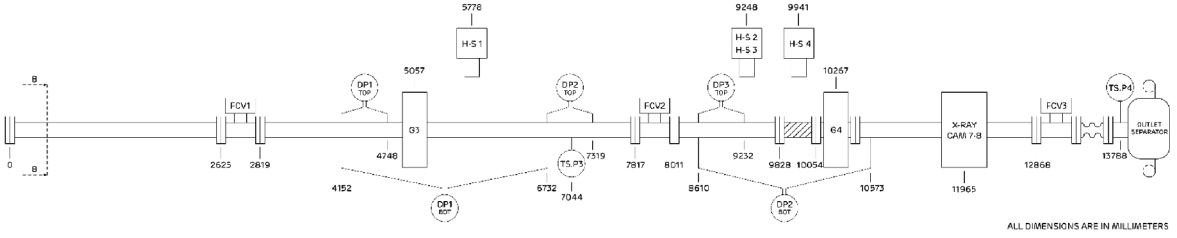

Fig. 4. Schematic of inclined Flow loop, HS = high-speed camera, G = Gamma densitometer, DP = Differential pressure transducer.

established mixture rule (Eq. (2)).

Lastly, A necessary modification to interFoam is introduced for the inclined simulations. InterFoam imposes a pressure discontinuity between periodic boundaries in an inclined domain due to the way gravity is included in the pressure equation.

$$p_d = p - \overline{\rho}\mathbf{g}\cdot\mathbf{x}, \tag{7}$$

$$\nabla p_d = \nabla p - \overline{\rho}\mathbf{g} - \mathbf{g}\cdot\mathbf{x}\nabla\overline{\rho}, \tag{8}$$

where $\mathbf{x}$ is the position vector. As is shown in Eqs. (7) & (8) there is a gravity term within the pressure equations. This gravity term creates a discontinuity for the periodic boundary condition between the inlet and outlet when the domain is inclined. In order to rectify this discontinuity, the boundary condition and momentum equation specification must be re-written from the modified pressure (p_d) to p, and the momentum equation must be further amended by adding the hydrostatic component back into the equation as a separate term. For a more thorough description of interFoam, the thesis by Rusche (2002) and Berberovic (2010) are the most complete descriptions of the solver that are publicly available.

4. Experimental setup

The experimental flow loops at IFE consists of a 50 and 15 m long loop in the horizontal and inclined configurations. The gas and liquid inlets are separated by a thin sheet which acts as a flow straightener, and the interior cylinder is held in place by spokes. The spokes and flow straighteners represent two geometrical elements that are not modeled in the simulations, and introduce some uncertainty to the experimental results through flow disturbances.

Along the test section, there are 3 broad-beam gamma densitometers (G) and 5 differential pressure transducers (DP). The gamma densitometers acquire holdup data at 50 Hz by measuring the incident beam attenuation. Using the fluid properties and attenuation coefficient, the liquid holdup within the test section is solved through Eq. (9) and (10). The intensity (γ) of an incident beam (γ_o) after passing through a fluid is

$$\gamma = \gamma_o exp(-\mu t), \tag{9}$$

where μ is the attenuation coefficient, and t the beam travel distance. For two-phase flows, the average cross-sectional holdup is calculated by

$$\alpha_l = \frac{log\left(\frac{\gamma_m}{\gamma_g}\right)}{log\left(\frac{\gamma l}{\gamma_g}\right)}. \tag{10}$$

The ratio of the calibrated single-phase gamma intensities (γ_g,γ_l) and measured gamma intensity (γ_m) are used to calculate the liquid holdup within the test section. Single-phase measurements of the beam attenuation are used to determine the calibrated intensities through Eq. (9). The radiation intensity of the original incident beam is reduced exponentially as a function of the fluid thickness, distance traveled, and attenuation coefficient. The measurement gamma intensity is determined through the beam attenuation of the two-phase experiments.

5. Fluid properties and mixture velocities

The fluid properties and mixture velocities are reflected in the simulations as initial conditions and as a momentum-source (mixture velocity). The average pressure gradient over each measurement interval can vary, and for cases where the holdup fraction on either side of the pressure gradient measurement varies significantly an average of the readings are used for the simulations. Therefore, the initialized holdup fraction of the simulation may be slightly different from the values recorded in Table 1, which in turn will affect the simulated pressure gradient. For example, case #1; one measuring station has an average of 63% holdup while the next has 58.5%.

Table 1
Liquid holdup fraction, mixture velocity and superficial liquid velocity.

Case #	α	U_{mix} (m/s)	u_{sl} (m/s)
1	0.63	1.2	0.2
2	0.45	2.7	0.2
3	0.48	4.2	1.2
4	0.53	4.1	1.6
5	0.44	2.25	0.25
6	0.53	2.75	0.75
7	0.43	3.75	0.75
8	0.46	4.25	0.75
9	0.30	2.25	0.25
10	0.40	2.75	0.75
11	0.32	3.75	0.75
12	0.46	3.25	1.25

Table 2
Summary of fluid properties for cases 1–4 with sulphur hexafluoride (gas) and Exxsol D60 (liquid) in a horizontal eccentric annulus (E = 1.0).

Case #	ρ_l ($\frac{kg}{m^3}$)	ρ_g ($\frac{kg}{m^3}$)	ν_l ($\frac{m^2}{s}$)	ν_g ($\frac{m^2}{s}$)
1	801.3	24.2	$1.75{\cdot}10^{-6}$	$6.19{\cdot}10^{-7}$
2	801.1	24.3	$1.75{\cdot}10^{-6}$	$6.17{\cdot}10^{-7}$
3	803.0	25.7	$1.74{\cdot}10^{-6}$	$5.83{\cdot}10^{-7}$
4	802.1	26.4	$1.75{\cdot}10^{-6}$	$5.69{\cdot}10^{-7}$

Table 3
Summary of fluid properties for cases 5–8 with sulphur hexafluoride (gas) and Exxsol D60/Marcol 82 mixture (liquid) in a 4° inclined eccentric annulus (E = 1.0).

Case #	ρ_l ($\frac{kg}{m^3}$)	ρ_g ($\frac{kg}{m^3}$)	ν_l ($\frac{m^2}{s}$)	ν_g ($\frac{m^2}{s}$)
5	854.1	43.8	$2.61{\cdot}10^{-6}$	$3.42{\cdot}10^{-7}$
6	854.3	43.9	$2.62{\cdot}10^{-6}$	$3.42{\cdot}10^{-7}$
7	854.4	43.9	$2.62{\cdot}10^{-6}$	$3.42{\cdot}10^{-7}$
8	856.1	44.0	$2.62{\cdot}10^{-6}$	$3.41{\cdot}10^{-7}$

Table 4
Summary of fluid properties for cases 9–12 with sulphur hexafluoride (gas) and Exxsol D60/Marcol 82 mixture (liquid) in a vertical eccentric annulus (E = 1.0).

Case #	ρ_l ($\frac{kg}{m^3}$)	ρ_g ($\frac{kg}{m^3}$)	ν_l ($\frac{m^2}{s}$)	ν_g ($\frac{m^2}{s}$)
5	854.3	44.8	$2.60{\cdot}10^{-6}$	$3.35{\cdot}10^{-7}$
6	855.3	45.1	$2.62{\cdot}10^{-6}$	$3.32{\cdot}10^{-7}$
7	855.6	45.0	$2.61{\cdot}10^{-6}$	$3.33{\cdot}10^{-7}$
8	857.4	45.5	$2.61{\cdot}10^{-6}$	$3.30{\cdot}10^{-7}$

In addition to the summarized data in Table 1, the surface tension coefficient is 0.0285 N/m. The fluids used during the horizontal (1–4) and inclined (5–12) experiment cases[1] are all the same, but due to system pressure, the density and viscosity vary slightly as summarized in Tables -2–5. In addition, simulation cases 13–16 are composed using the basic information from experiment cases 5–8, in order to study the effect of an increased inclination.

[1] cases 1–12 correspond to experiment # 6005, 6008, 6089, 6106, 7048, 7053, 7054, 7059, 7185, 7190, 7191 and 7195 in the IFE database

Table 5
Liquid holdup fraction, mixture velocity and superficial liquid velocity.

Case #	f	h/d_h	regime
1	0.25	0.60	I
2	0.63	0.46	I
3	0.76	0.49	I
4	0.63	0.52	I
5	0.61	0.45	I
6	0.61	0.52	I
7	0.91	0.45	I
8	1.06	0.47	I/DB
13	0.61	0.45	I
14	0.61	0.52	I
15	0.92	0.45	I
16	1.07	0.47	I/DB

6. Flow regime prediction

There are only a few mechanistic models that can be applied uniformly to the 16 cases analyzed in the present work. One of these models is a unified model proposed in Shoham (2006) and builds upon models established by Taitel and Dukler (1976) and Barnea (1987). The proposed unified model is applicable for the full range of inclinations studied in this article and can be utilized to predict the flow regime of all cases. However, the model was originally intended for hollow pipes, and may therefore be sensitive to geometrical influences. In particular, this unified model is heavily dependent on the liquid height. Due to the interior cylinder, the liquid height in an annulus is drastically different than it would be in a hollow pipe. The reader should also note that the Barnea and Taitel models were designed the using units lbf, lbm and ft. Because there are no available unified models for flow regime prediction developed specifically for an annulus geometry, the proposed unified model represents one of the better methods for flow regime prediction. For a thorough description of the unified flow regime prediction model, the book by Shoham (2006) or publication by Gomez et al. (1999) offer an in-depth description of the model and the underlying methodology.

The Barnea unified model works under the assumption that there are 5 distinct flow regimes, Stratified (SS), intermittent (I), bubble (B), dispersed bubble (DB) and annular (A) flow. Because some flow regimes, such as churn flow, predominantly occur at very high inclinations, it is considered part of the intermittent regime of the unified model. Stratified-wavy (SW) was another flow regime, which was not included in the model but is considered a sub-regime of the stratified flow regime. The solution procedure can be summarized in a few simple steps. First determine the dimensionless parameters which depend on the geometry and fractional holdups. Thereafter using these dimensionless parameters, check the transition criteria sequentially for stratified to intermittent flow, intermittent to annular flow, and intermittent to bubbly and dispersed bubbly flow.

We compare the expected flow regimes from both the Taitel flow regime map and Barnea unified model, which is presented in Shoham (2006). The flow regime map by Taitel was created using a similar approach as the Barnea model, but is only applicable to a small range of inclinations from horizontal to inclined flows up to 10°. Further, the flow regime map only requires the calculation of the Froude number and a dimensionless number referred to as the equilibrium liquid height ($\widetilde{h_L}$), which is the liquid level (h_L) divided by the hydraulic diameter (d_h) to be utilized.

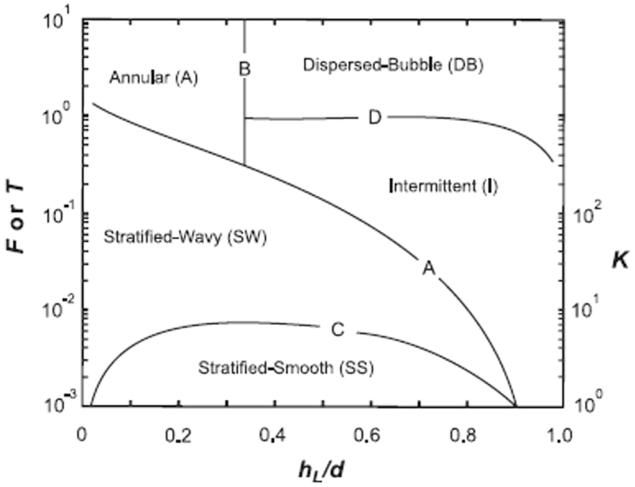

Fig. 5. Generalized flow regime map for horizontal and near horizontal inclinations, adapted from Taitel and Dukler (1976).

$$\widetilde{h_L} = \frac{h_L}{d_h}. \tag{11}$$

The equilibrium liquid height (Eq. 11) is determined using geometry assuming an equivalent hydraulic diameter for a hollow pipe. Together with $\widetilde{h_L}$, the Froude number (F), modified by the density ratio (Eq. 12) determines the transition points for the flow pattern map.

$$F = \sqrt{\frac{\rho_g}{\rho_L - \rho_g}}\,\frac{u_{sg}}{\sqrt{d_h g cos\theta}}, \tag{12}$$

where, the subscript s symbolizes superficial velocity. Calculating the two dimensionless numbers, the generalized flow regime map for horizontal and near horizontal inclinations (Fig. 5) can be utilized to predict the expected flow regimes for cases 1–8 and 13–16.

As described by the plotted data (Fig. 5), based on the generalized flow regime map, the expected flow regime for all low inclination cases are predicted as an intermittent flow regime except cases 8 and 16 which are on the transition line between dispersed bubbly and intermittent. In addition to cases 8 and 16, cases 1,2, and 5 are relatively close to the stratified wavy transition line. Due to the uncertainty caused by the annulus geometry when utilizing a flow regime model based on hollow pipes, we consider that these cases may be wavy.

In order to predict the remaining vertical cases, the full Barnea model, which is applicable from −90° to 90° is applied, and the low inclination cases were re-tested with this model. However, due to the similarities of the models, the expectation is that the low inclination cases will remain intermittent.

Please note that the transition test procedure must be done sequentially and in a specific order (Shoham, 2006). The test criteria is summarized below. If the reader is interested in a more in-depth description, Shoham (2006), Gomez et al. (1999) and Barnea (1987) are appropriate resources. The first transition point that the Barnea model analyzes is the stratified to intermittent transition. The criterion for the Barnea model is derived from a Kelvin–Helmholtz stability analysis and is also the same criterion utilized to create the transition boundary from stratified to intermittent in the Taitel flow regime map (Fig. 5).

$$F^2\left[\frac{1}{\left(1-\widetilde{h}_L\right)^2}\frac{\widetilde{u}_g^2\widetilde{S}_I}{\widetilde{A}_g}\right]\geqslant 1 \tag{13}$$

where $\widetilde{S}_I = \sqrt{1-(2\widetilde{h}_L-1)^2}$, $\widetilde{u}_g = \frac{u_g}{u_{sg}}$, and $\widetilde{A}_g = A_g/d_h^2$, and A_g is the cross-sectional area occupied by gas in the equilibrium state. If Eq. (13) is not true, then further analysis can establish whether the flow is stratified wavy. If the relationship is true, then the flow is either intermittent, bubbly, or annular. The next transition point considered is intermittent to dispersed bubbly. This transition requires the calculation of 4 terms for inclinations below 10° and 3 terms for higher inclinations.

The first term is the void fraction. In the unified model, the transition from intermittent to dispersed bubbly flow can only occur if the void fraction is less than 0.52 (Shoham, 2006), expressed as

$$1-\alpha < 0.52, \tag{14}$$

where α is the liquid holdup.

The unified model, proposes solving the void fraction by

$$\alpha_g = \frac{u_{sg}}{u_{sl}+u_{sg}} \tag{15}$$

If the void fraction is less than 0.52, the remaining transition criteria from intermittent to dispersed bubbly can be performed. The value of 0.52 is significant because it is the theoretical maximum packing of bubbles. Above this void fraction bubble agglomeration occurs, causing slug or intermittent flow (Gomez et al., 1999). After the void fraction criteria is passed, the maximum (d_{max}, Eq. 16) and two critical bubble diameters (d_{cd} & d_{cb}, Eqs. 17 & 18) are established. For the cases presented in this paper, both Eq.(15), and the measured void fraction was checked, and if either qualified for the criterion, we performed the transition tests. It should be noted, that this particular void fraction equation quite drastically overestimated the measured void fraction.

$$d_{max} = \left[0.725+4.15\left(\frac{u_{sg}}{u_m}\right)^{0.5}\right]\left(\frac{\sigma}{\rho_L}\right)^{0.6}\left(\frac{2f_m u_m^3}{d_h}\right)^{-0.4} \tag{16}$$

$$d_{cd} = 2\left[\frac{0.4\sigma}{(\rho_L-\rho_g)g}\right]^{0.5} \tag{17}$$

$$d_{cb} = \frac{3}{8}\frac{\rho_L}{(\rho_L-\rho g)}\frac{f_m u_m^2}{g cos\theta} \tag{18}$$

The transition to dispersed bubble flow occurs for low inclination flows when $d_{max} < d_{cd}\, and\, d_{cb}$, while it occurs for high inclination flows when $d_{max} < d_{cd}$ (Shoham, 2006).

The transition from annular to intermittent flow has two requirements, instability of the film near the wall and the liquid holdup (Gomez et al., 1999). Due to the formulation, the flow will remain intermittent if either condition is satisfied. The first condition is very straight forward, and states that there will not be annular flow if

$$\alpha > 0.24, \tag{19}$$

This condition coincides with the low inclination flow regime map (Fig. 5). At inspection, the transition (B) from the intermittent to annular flow regime occurs at $h_L/d_h \approx 0.35$, which equates to a liquid holdup of 0.25 which holds true for all of the vertical cases studied here. For the other transition requirement, the reader can refer to Shoham (2006) and Gomez et al. (1999).

The final transition considered in the unified model is the transition to bubble flow, which is separate from dispersed bubble flow, and occurs only below a critical void fraction of 0.25 and when the inclination is between 60 and 90°. Typically, the solution procedure given in Shoham (2006) requires the numerical solution of the void fraction; however, since the void fraction within our vertical domains is known, and it is always above 0.25, the cases are not expected to be bubble flow. At void fractions above 0.25, there is bubble agglomeration and transition to an intermittent flow.

$$u_{sL} = \frac{1-\alpha_g}{\alpha_g}u_{sg} - 1.53\left(1-\alpha_g\right)^{0.5}\left[\frac{g(\rho_L-\rho g)\sigma}{\rho_L^2}\right]^{1/4} sin\theta \tag{20}$$

When following the uniform model approach by numerically solving the void fraction based on the above relationship, the void fractions are within 0.2 of the measured void fractions, and well above the critical void fraction of 0.25. Based on the unified model, the 4 vertical cases

Table 6
Summary of Wave and slug frequencies for horizontal eccentric experiment cases (E = 1.0), with sulphur hexaflouride (gas) and Exxsol D60 (liquid).

Case #	Slug frequency (Hz)	Wave frequency (Hz)
1	–	0.49
2	–	0.65
3	1.16	–
4	1.72	–

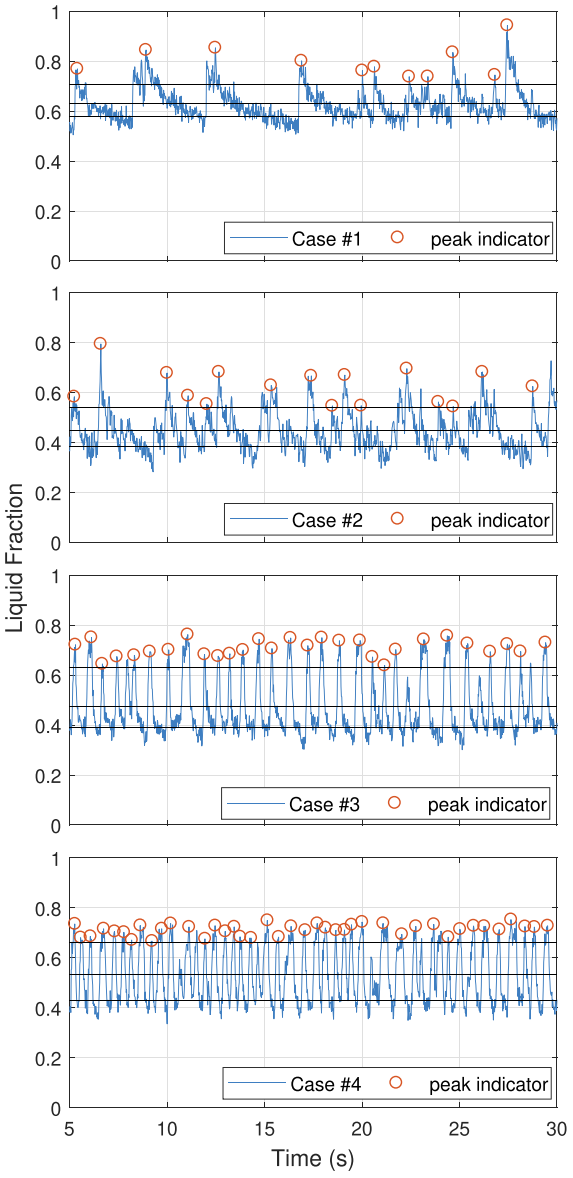

Fig. 6. Experimental liquid holdup as a function of time for horizontal eccentric annulus (E = 1.0) cases 1–4 with sulphur hexaflouride (gas) and Exxsol D60.

should all be intermittent flow.

As described above, the analysis suggests that all cases satisfy the conditions for intermittent flow. In the vertical cases, this may be churn flow as it is included in the intermittent phase. It is also possible to construct specific flow regime maps using the above relationships. In order to do so, several closure relationships are required. If the reader is interested in doing so Shoham (2006) contains an in-depth explanation of the procedure.

7. Summary of experimental results

The experimental results are split into three categories; horizontal (1–4), 4° (5–8), and 90° (9–12). The phase fractions and mixture velocities extracted from the experiments are utilized in the simulations to initiate and drive the flow (mixture velocity). Allowing the pressure gradients (Pa/m) and holdup transients to be simulated. In the following section, the slug and wave frequency of each case as well as the pressure gradient measured at the 4th DPT location are shortly summarized in order to give context to the computational results.

The entirely eccentric horizontal cases (1–4) summarized in Table 6 and shown in Fig. 6, consist of two wavy and two slug cases. The slug identification procedure follows the method outlined in Nuland (1999) and is built on utilizing thresholds to determine Taylor bubble and slug occurrences. Case 1 exhibits a few large long-period waves separated by a relatively calm state. Each successive case afterward has an increased frequency of waves or slugs, corresponding to an increased mixture velocity (Table 1). To confirm the flow regime of each case, visual data recorded at the third high-speed camera location 37 m downstream of the inlet is cross-referenced.

Each snapshot shown in Fig. 7, represent the case's dominant flow regime. Case #1, exhibits a few large waves separated by a region of calmer flow. Case #2 is dominated by large waves of varying amplitude, with significantly more phase mixing than Case #1, as shown by the darkening of the liquid. The darkening effect occurs when gas bubbles permeate throughout the liquid, also noticeable in the two slug cases (3 & 4). The two slug cases show an emerging slug (Case #3) together with the calmer region in front, and the Taylor bubble (Case #4) separating two slugs.

Table 7 summarizes the pressure gradient transients (Fig. 8) for cases 1–4. The three values recorded correspond to two threshold values (95 and 5%) and the mean pressure gradient. The two thresholds are defined, such that 5% of the data is below the minimum threshold and

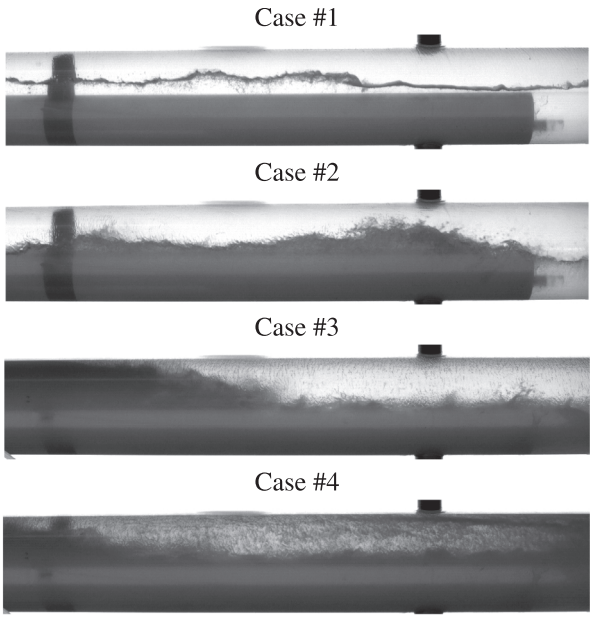

Fig. 7. Snapshots of flow regime for horizontal eccentric annulus experiments.

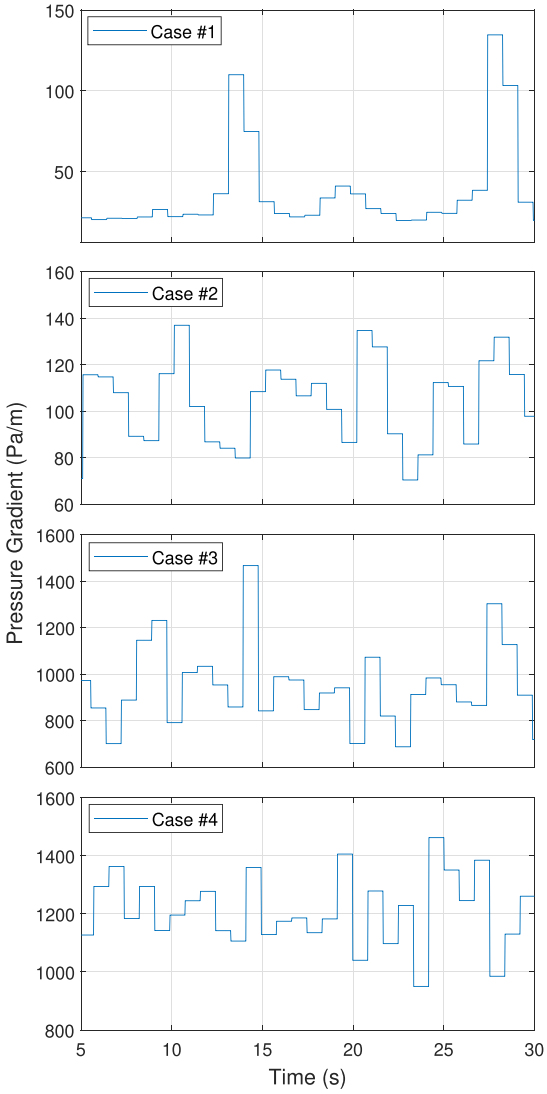

Fig. 8. Experimental pressure gradient as a function of time for horizontal eccentric annulus (E = 1.0) cases 1–4 with sulphur hexaflouride (gas) and Exxsol D60 (liquid).

Table 7
Pressure gradient summary for horizontal eccentric annulus experiment cases (E = 1.0) with sulphur hexaflouride (gas) and Exxsol D60 (liquid)..

Case #	5% (Pa/m)	mean (Pa/m)	95% (Pa/m)
1	15.29	36.27	98.20
2	74.90	102.95	136.95
3	696.43	961.00	1332.89
4	1031.45	1207.22	1405.03

Table 8
Summary of Wave and slug frequencies for 4° inclined eccentric annulus experimental cases (E = 1.0) with sulphur hexafluoride (gas) and Exxsol D60/ Marcol 82 mixture (liquid).

Case #	Slug frequency (Hz)	Wave frequency (Hz)
5	–	0.58
6	0.83	–
7	0.98	–
8	1.27	–

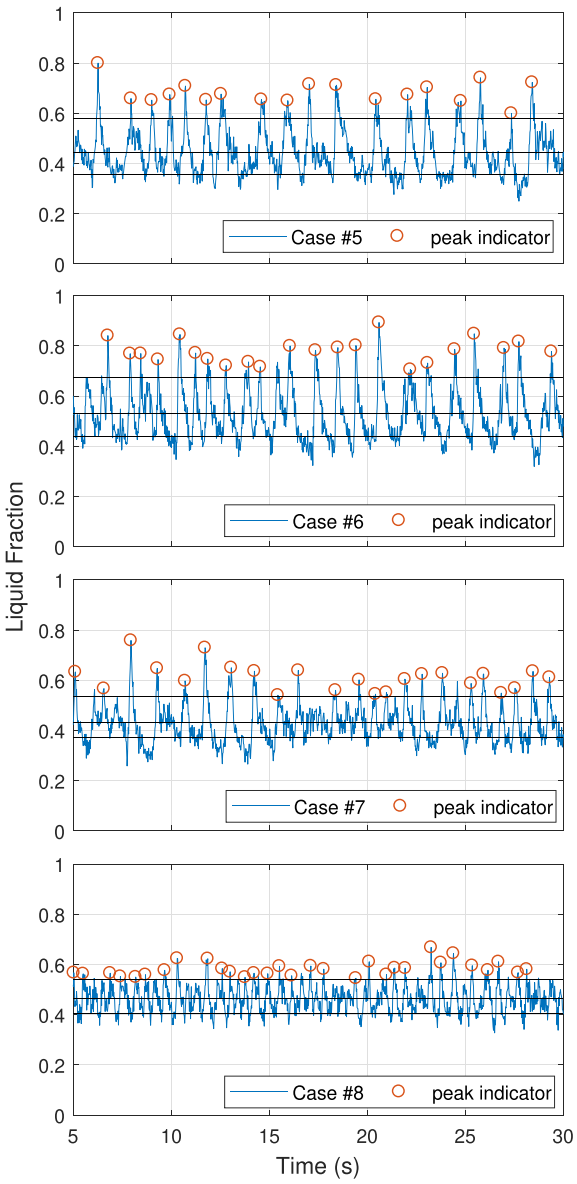

Fig. 9. Experimental liquid holdup fraction as a function of time for eccentric annulus (E = 1.0) cases 5–8 at 4° inclination with sulphur hexafluoride (gas) and Exxsol D60/Marcol 82 mixture (liquid).

5% above the maximum threshold. In general, the pressure gradient increases with increasing mixture velocity and with liquid holdup (Table 1); Case 4 has a 0.1 m/s lower mixture velocity compared to case 3, however, the pressure gradient is higher, in part due to a 0.05 fractional holdup increase. There is also a significant increase of several hundred Pa/m between the wave and slug flow cases.

The flow regime of the inclined cases (Table 8) is more complicated to analyze due to the increased amount of mixing, as shown by the darker images in Fig. 10; Case #5 is most likely dominated by large waves. The remaining three cases (6–8) are all likely slug cases, with some uncertainty with regards to case #8 due to the low peak holdup (Fig. 9); however, the combination of significant aeration and high-pressure gradient (Table 9) indicates case 8 is probably a high-frequency slug flow.

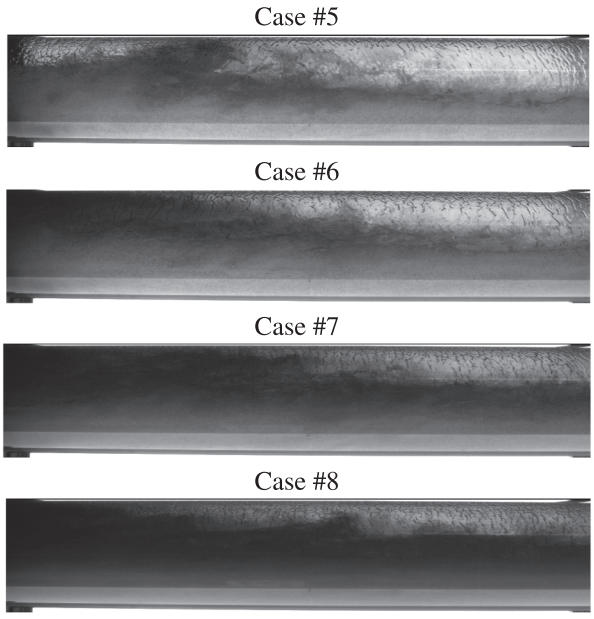

Fig. 10. Snapshots of flow regime for 4° inclined eccentric annulus experiments.

Table 9
Pressure gradient summary for 4° inclined eccentric annulus experimental cases (E = 1.0) with sulphur hexaflouride (gas) and Exxsol D60/ Marcol 82 mixture (Liquid).

Case #	5% (Pa/m)	mean (Pa/m)	95% (Pa/m)
5	261.4	497.2	802.7
6	645.6	1018.7	1375.5
7	850.9	1188.3	1612.3
8	1616.3	1791.0	1956.4

The most noticeable differences between the horizontal and 4° inclined cases (Figs. 7 & 10) is the increased darkening of the liquids in the inclined cases and increased pressure gradient when the holdup fractions and mixture velocities are similar. The leading cause for the darkening is the increased mixing caused by the higher mixture velocity and inclination. The inclination also introduces strong shear flows through backflow in the lower liquid layer, most prominent in cases 5 and 6. Carefully inspecting the case images, small gas bubbles are visible; by following the bubbles in a series of images counter-current flow (backflow) is observed.

Case #5 (Fig. 11), which is at 0.45 m/s lower U_{mix} than horizontal case #2 (Table 1) and nearly identical holdup, has an almost 5 times higher pressure gradient (Tables 7 & 9). The increased pressure gradient shows the pronounced effect of inclination on the pressure gradient caused due to the static head. From the respective holdup profiles (Figs. 6 & 9), we also notice that the flow regime is affected by inclination. The inclined flow is a wavy flow or perhaps a slug flow with a clear periodic trend, while the horizontal case is wavy with a less defined wave-period. As with the horizontal cases (Table 7), there are also clear pressure gradient trends with respect to mixture velocity and fractional holdup (Table 1) for the 4° inclined cases (Table 9).

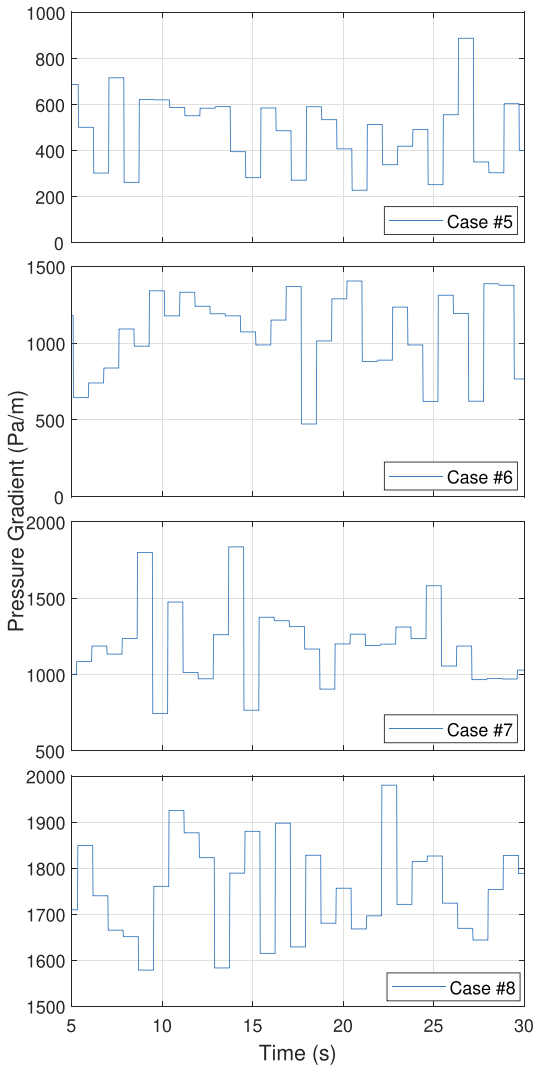

Fig. 11. Experimental pressure gradient as a function of time for eccentric annulus (E = 1.0) at 4° inclination with sulphur hexaflouride (gas) and Exxsol D60/ Marcol 82 mixture (Liquid).

Table 10
Holdup peak frequency for 90° inclined eccentric annulus experimental cases (E = 1.0), with sulphur hexafluoride (gas) and Exxsol D60/Marcol 82 mixture (liquid).

Case #	Frequency (Hz)
9	1.71
10	1.94
11	1.69
12	2.48

The frequencies identified for the 90° inclined eccentric annulus flow (Table 10) are obtained in the same way as for the wave and slug cases for the horizontal and 4° cases. However, the frequencies represent holdup peaks of the churn/wispy annular flow. All of the vertical cases are significantly harder to analyze due to the extreme amount of mixing and

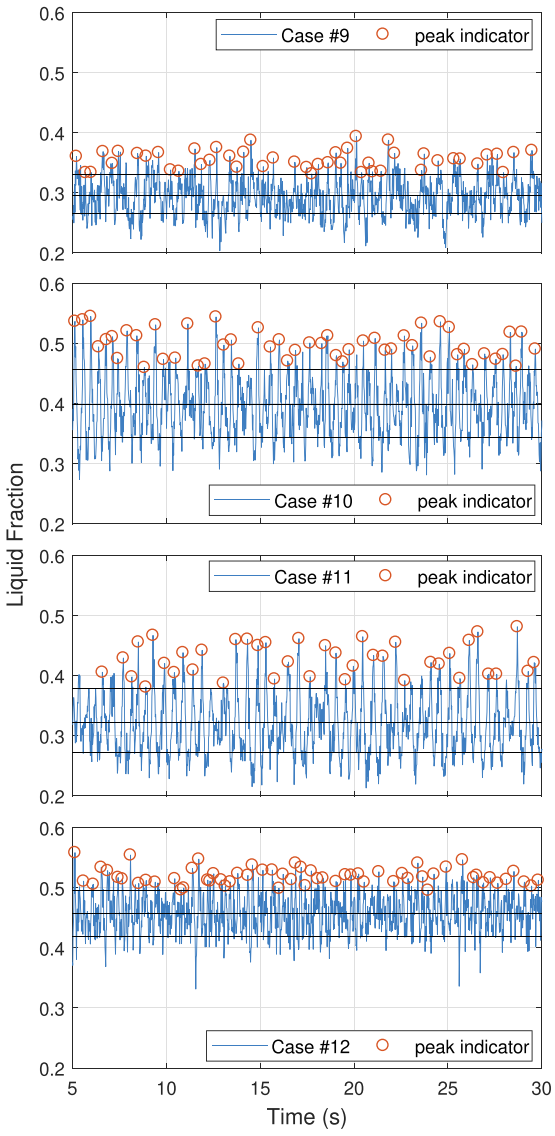

Fig. 12. Experimental liquid holdup as a function of time for eccentric annulus (E = 1.0) cases 9–12 with sulphur hexafluoride (gas) and Exxsol D60/Marcol 82 mixture (liquid).

liquid covering of the outer cylinder walls (Fig. 13). Therefore, flow regime identification is based on the liquid holdup (Fig. 12). Because the holdup is predominantly within the region of 30–50%, which is too high for conventional annular flow, and the walls are wetted by liquid, we believe the cases are most likely churn flow. There is also a possibility that the flow observed is a type of wispy annular flow with elongated bubbles of liquid within a gas core. In this case, the inside is presumably dominated by a gas core with flakes of liquid passing up through the gas layer.

The outer cylinder wall for cases 9–12 is covered in a liquid film (Fig. .13). The lighter regions are either sections where the liquid film very thin or wholly removed; most likely thin layers. The liquid film is observed moving slowly upward through a time-lapse; however, near the contact line between the interior cylinder wall and outer cylinder wall, there is a region of backflow. When backflow collides with a counter-directional flow, it may splash out into the interior and follow

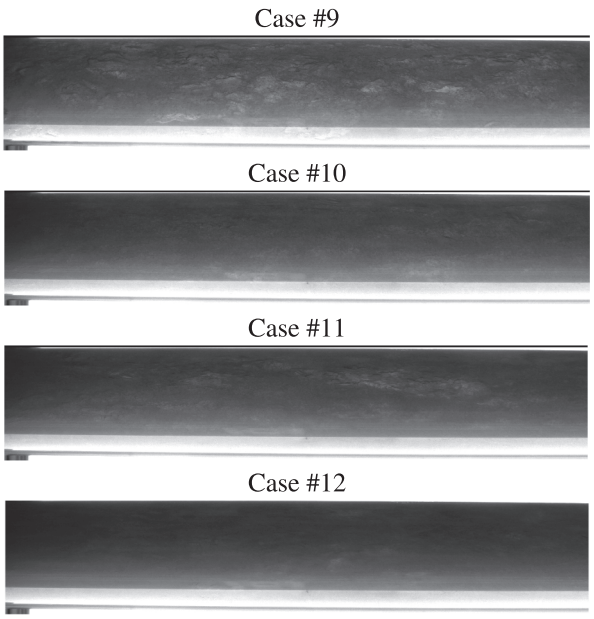

Fig. 13. Snapshots of flow regime for 90° inclined eccentric annulus experiments.

Table 11
Pressure gradient summary for 90° inclined eccentric annulus experimental cases (E = 1.0) with sulphur hexafluoride (gas) and Exxsol D60/Marcol 82 (liquid).

Case #	5% (Pa/m)	mean (Pa/m)	95% (Pa/m)
9	2281.0	2440.8	2586.7
10	3846.6	4054.7	4215.4
11	3357.4	3606.7	3857.1
12	5198.9	5274.1	5345.1

the core upwards. There are also regions where the liquid oscillates up and down, which is typical of churn flow.

The spread of the pressure gradient data is modest, with the vast majority of data points being within ±5% of the mean (Table 11 & Fig. 14). For churn flow, the pressure gradient is expected to be lower when large gas bubbles pass through the test section, and higher when the test section is mostly filled with liquid. The DPT test sections are approximately 1 m long, which may smear that data, therefore the pressure gradient data alone is insufficient to distinguish the potential flow regimes, and we will continue to classify the flow in the experimental cases 9–12 as churn flow.

Compared to the unified model and flow regime map, the experimental data agrees with the small caveat of cases 1,2 and 5. The experimental data indicates that these are wavy flows, while the flow regime map and unified flow model both predict intermittent flows. Small discrepancies are to be expected when using a model not distinctly designed for the geometry studied in this, and cases 1, 2 and 5 are as noted very close to the transition line between stratified wavy and intermittent flow.

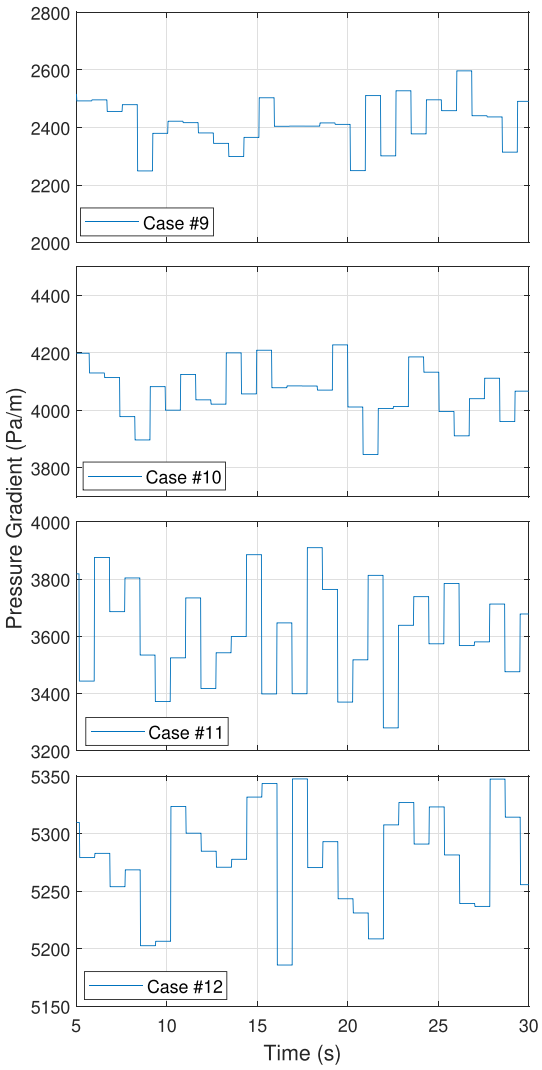

Fig. 14. Experimental Pressure gradient as a function of time for vertical eccentric annulus (E = 1.0) cases 9–12 with sulphur hexafluoride (gas) and Exxsol D60/Marcol 82 (liquid).

8. Simulation results

The experimental fluid properties, average holdup, and mixture velocities are extracted in order to initiate and drive the simulations. Simulation cases 13–16 are a replica of cases 5–8 at an increased inclination in order to study the effect of a small change of inclination. The fluid properties of each case mirrors the experimental cases and can be reviewed in Tables 1–4. The results are separated into four categories; horizontal, 4°, 90°, and 10° inclination. Following the established structure, the holdup results and key numbers are presented followed by the pressure gradient results. The solver used for the inclined simulations is a modified interFoam.

8.1. Simulated pressure gradient and holdup fraction results for horizontal eccentric annulus (E = 0.98) cases 1–4 with sulphur hexafluoride (gas) and Exxsol D60 (liquid).

Compared to the predicted flow regime using a unified model, the horizontal cases are in agreement for cases 3 and 4. Correspondingly, based on the holdup transients, the horizontal cases (Fig. 15) are in reasonable agreement with their experimental counterparts (Fig. 6), especially case 1, which is dominated by low-frequency waves. The three remaining horizontal cases are better compared through the simulation (Table 12) and experiment (Table 6) peak frequency. The key

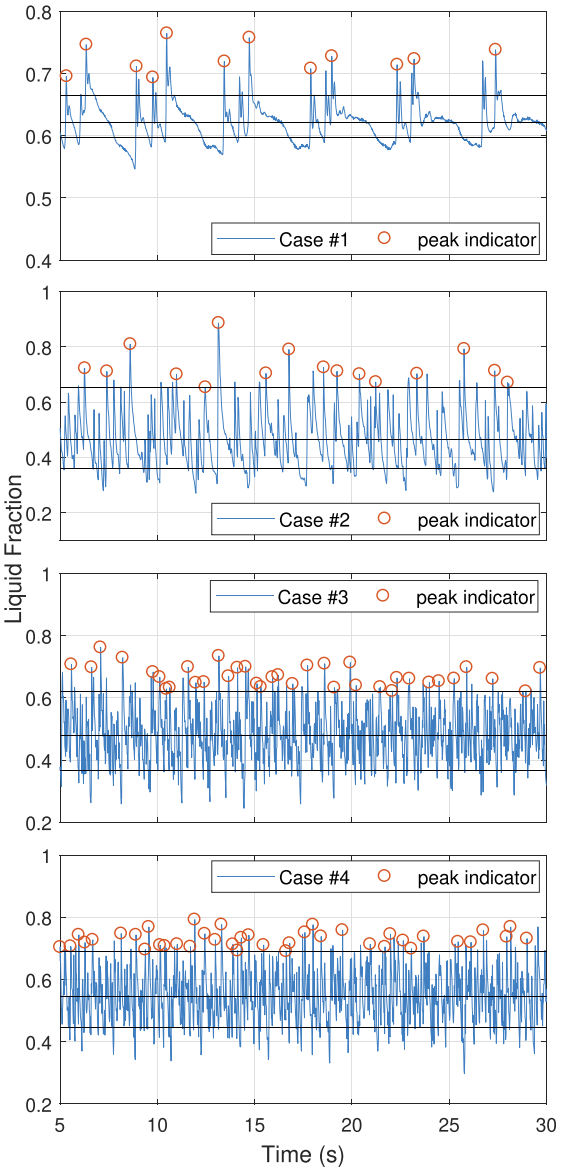

Fig. 15. Simulated liquid holdup fraction for horizontal eccentric annulus (E = 0.98) with sulphur hexaflouride (gas) and Exxsol D60 (liquid).

Table 12
Simulated wave and slug frequencies for horizontal eccentric (E = 0.98) cases 1–4 with sulphur hexaflouride (gas) and Exxsol D60 (liquid).

Case #	Slug frequency (Hz)	Wave frequency (Hz)
1	–	0.48
2	–	0.64
3	1.44	–
4	1.60	–

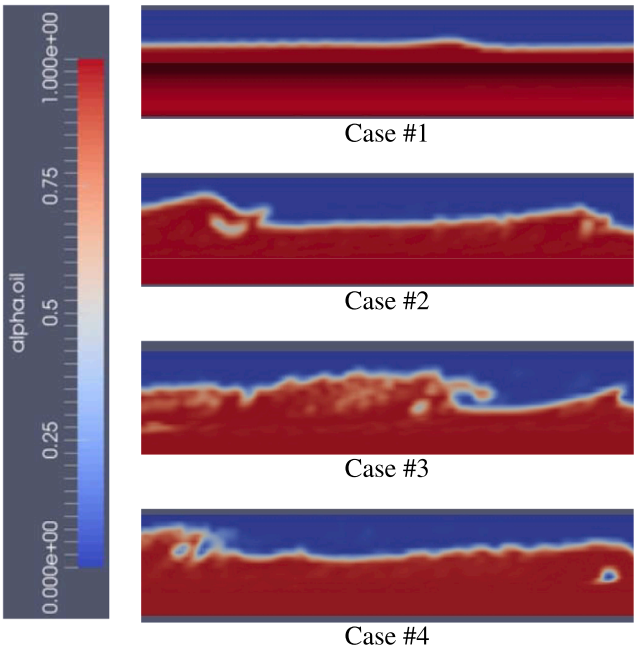

Fig. 16. Snapshots of flow regime for horizontal eccentric annulus simulations.

figures shows that the frequencies are within 0.3 Hz for all cases. Simulation cases 1 (wave), 3 (slug), and 4 (slug) appear to share a flow regime with the experiments. In regards to case 2, the cross-sectional holdup peaks are in the region of 0.7, with a few peaks at 0.8 or higher in both experiment and simulation, however, the simulations could be a proto-slug. The experiment flow regime images (Fig. 7) are cross-referenced with the streamwise slices of the simulated flow field to more accurately determine the flow regimes.

The simulated cases exhibit a near-complete lack of minor gas bubbles entrapped within the liquid. When the mesh is incapable of resolving small bubbles, they coalesce to form large gas bubble, as shown in case 4 (Fig. 1617) or remain outside of the liquid layer. Other factors such as surface tension treatment and turbulence modeling could also affect bubble formation. As shown by the holdup profiles, the simulated liquid holdup peaks (Fig. 15) are in line with the experimental cases (Fig. 6); however, due to a lack of gas penetration into the liquid, there are no conventional slugs observed in the simulations (Fig. 16). Therefore, the simulated slug structures are referred to as proto-slugs, proto-slugs resemble a short conventional slug and may or may not develop into a persistent slug. The image for case 1 is captured at the symmetry line, while the remaining images are an interior slice.

The most noticeable pressure gradient discrepancies in comparison with the experiments occur for cases 1 and 2 (Tables 13 & 14). These are low velocity cases, and a possible reason for the discrepancy is how turbulence is handled and generated in a VOF solver combined with the k-*omega* RANS model. A VOF solver functions by using an averaged imaginary liquid, the procedure could artificially induce turbulence throughout the fluids, while experiments have less turbulence in the liquid. Another alternative is the pressure solutions sensitivity to wall effects. Based on previous simulation campaigns (Friedemann et al., 2019), the 115 k cells/m mesh and solution method often over-predicts the pressure gradient.

When the simulations at a reduced eccentricity from Friedemann et al. (2020) but identical in all other matters are compared to these results, the pressure gradients for the fully eccentric simulations are reduced by 30–40% for all cases except case 2. Caetano (1985) found that the single-phase pressure gradient ratio for an annulus at E = 0.5 to be roughly 0.45 of an equivalent hollow pipe, while a fully eccentric annulus was roughly

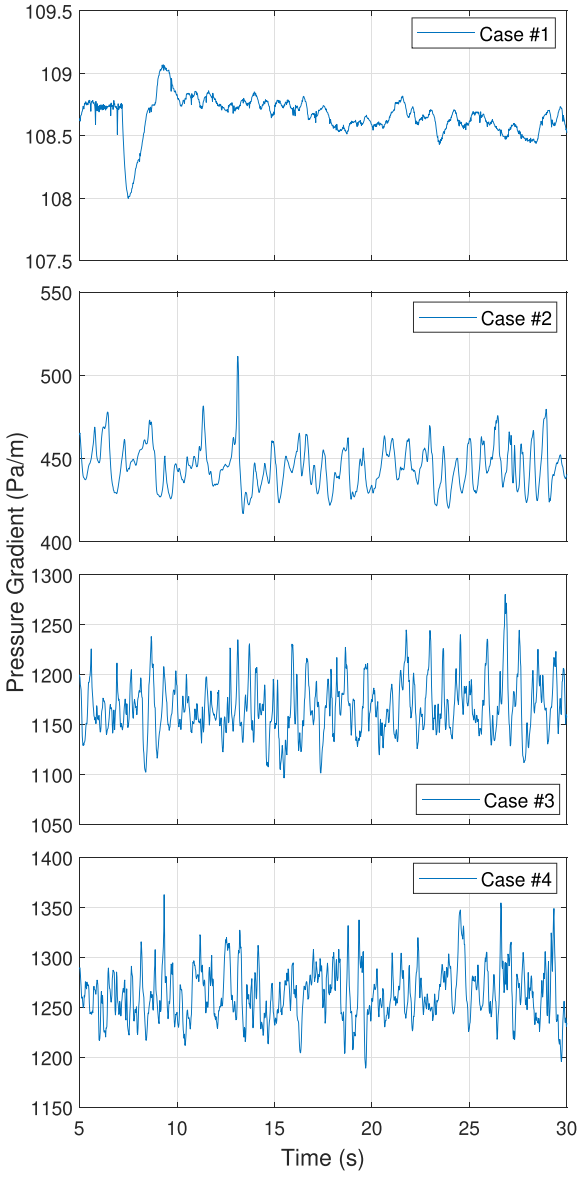

Fig. 17. Simulated pressure gradient as a function of time for horizontal eccentric annulus (E = 0.98) cases 1–4 with sulphur hexaflouride (gas) and Exxsol D60 (liquid).

Table 13
Simulated pressure gradient summary for horizontal eccentric annulus (E = 0.98) cases 1–4 with sulphur hexaflouride (gas) and Exxsol D60 (liquid).

Case #	5% (Pa/m)	mean (Pa/m)	95% (Pa/m)
1	108.5	108.7	108.8
2	425.9	445.1	467.8
3	1126.0	1167.5	1215.7
4	1223.8	1263.3	1307.9

Table 14
% difference between simulated pressure gradient and experimental pressure gradient for horizontal eccentric annulus simulation cases with E = 0.983.

Case #	5% (%)	mean (%)	95% (%)
1	610	196	10.7
2	469	332	242
3	61.7	21.5	−8.8
4	19.6	4.6	−6.9

Table 15
Simulated Wave and slug frequencies for 4° inclined eccentric annulus (E=.983) cases 5–8 with sulphur hexaflouride (gas) and Exxsol D60/ Marcol 82 mixture (Liquid).

Case #	Slug frequency (Hz)	Wave frequency (Hz)
5	–	1.04
6	1.36	–
7	1.24	–
8	1.72	–

0.25 of a hollow pipe for annulus with diameter ratios (D_i/D_o) of 0.5, in other words a 45% reduction of the pressure gradient as an effect of increasing the eccentricity from 0.5 to 1.0, while Ferroudji et al. (2019) found a decrease in pressure drop of roughly 17% when increasing the eccentricity from 0.6 to 0.9 for a power-law fluid or 25% when increasing from 0.3 to 0.9, also for a pipe diameter ratio of 0.5.

It is likely case #2 does not have a similar reduction due to the development of a different flow regime, with increased slug frequency in the previous publication. Compared to the experiments, the deviation

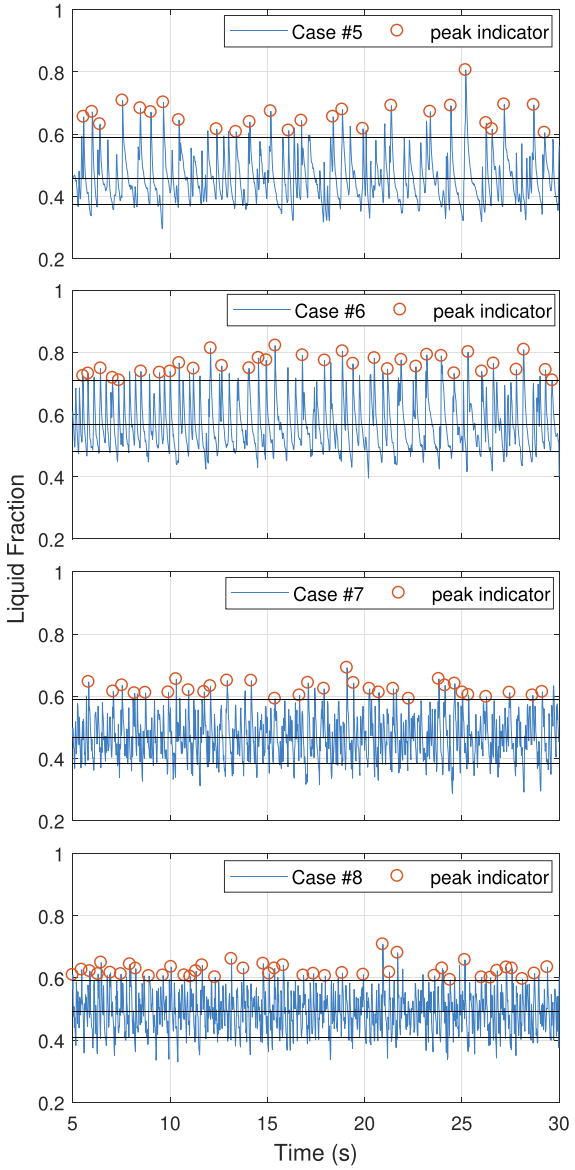

Fig. 18. Simulated liquid holdup fraction for eccentric annulus (E = 0.983) cases 5–8 at 4° inclination with sulphur hexaflouride (gas) and Exxsol D60/ Marcol 82 mixture (Liquid).

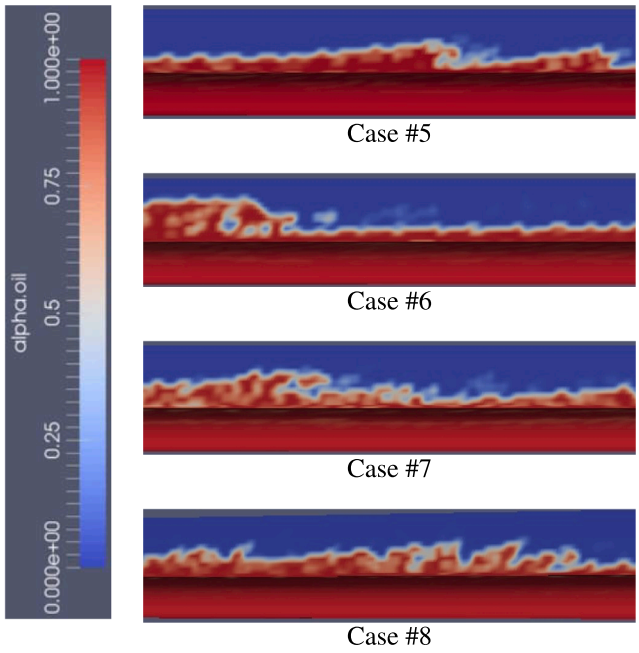

Fig. 19. Snapshots of flow regime for eccentric annulus simulations at 4° inclination.

from mean to either threshold is noticeably reduced. It will subsequently be shown that the relatively concentrated data persists for the inclined simulations. Compared to the experimental data, the simulated mean pressure gradient is within 4–22% for cases 3 and 4, while the two low velocity cases are off by 200–335%. There are several possible explanations for the over-prediction at low velocity cases, some of which were briefly mentioned, and needs to be further examined through other solution methods like an euler-euler multiphase approach, different wall functions, mesh densities, turbulence models or software such as Ansys Fluent.

8.2. Simulated pressure gradient and holdup fraction results for fully eccentric annulus (E = 0.983) at 4° inclination with sulphur hexaflouride (gas) and Exxsol D60/ Marcol 82 mixture (Liquid).

The wave and slug frequencies for cases 5–8 (Table 15) are consistently around 0.3–0.5 Hz higher than the experiments. Because the experiment time-series is 120 s, while the simulations are 30 s intervals with 25 s analyzed, some deviation is expected. For example, for the 25 s of experiment case 5 shown in Fig. 9 the wave frequency is 0.72 Hz, or 0.14 Hz higher than the data-set average, which indicates that even though there is a seemingly significant discrepancy, it is likely that within the full time-series there are periods where the simulations and experiments agree. The peak holdup for cases 5–8 (Fig. 18) are consistent with the experimental measurements (Fig. 9) with the exception the isolated holdup reading above 0.8 for experiment case #7. see Fig. 19-20.

Similarly to the horizontal cases (Fig. 16) there are no conventional slugs at 4° inclination (Fig. 10). Even when increasing the mesh density to 400 k cells/m no conventional slugs are produced. However, slugs are maintained for a prolonged period if they are part of the initial conditions, alternatively, created by initializing with a significantly lower

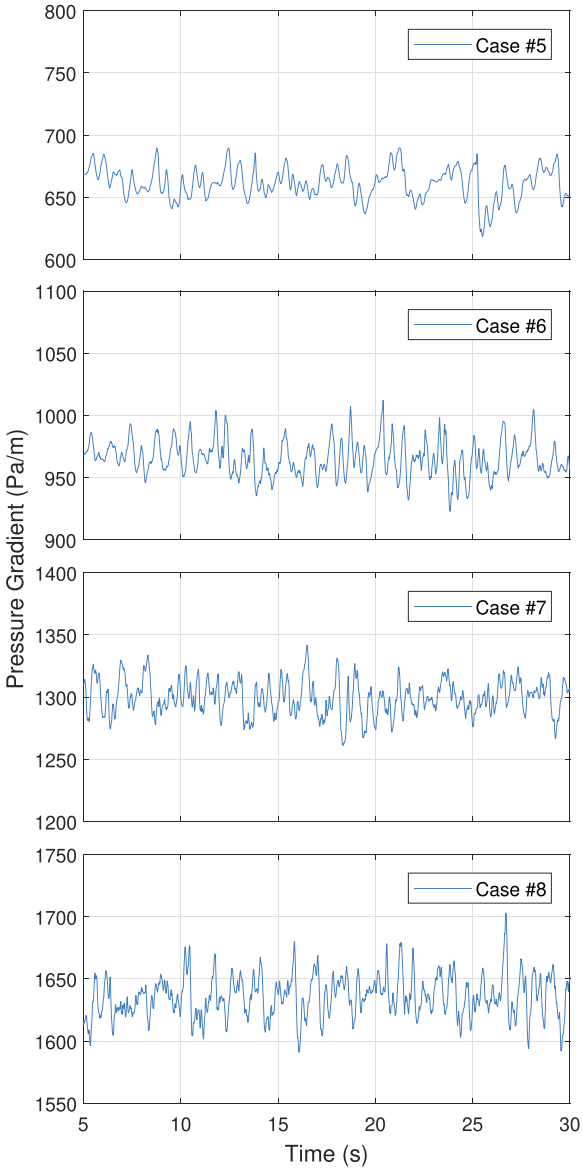

Fig. 20. Simulated pressure gradient as a function of time for an eccentric annulus (E = 0.983) at 4° inclination with sulphur hexaflouride (gas) and Exxsol D60/ Marcol 82 mixture (Liquid).

mixture velocity and then accelerating the flow. In both cases, the flow will eventually stabilize to the same proto-slug flow regime. The forced slugs which occur with the alternate initialization schemes are a transient occurrence. It is likely possible to achieve slug flow by altering the experimental surface tension. However, by altering the surface tension, the simulations are no longer attempted replicas of the experiments. see Fig. 24-28.

The lowest velocity case, case # 5 (Table 16 & 17), oscillates between 650 and 690 Pa/m. Remember that the horizontal cases that the simulations drastically over-predict the pressure gradient for the low velocity flows; however, the inclined simulations are likely in better agreement

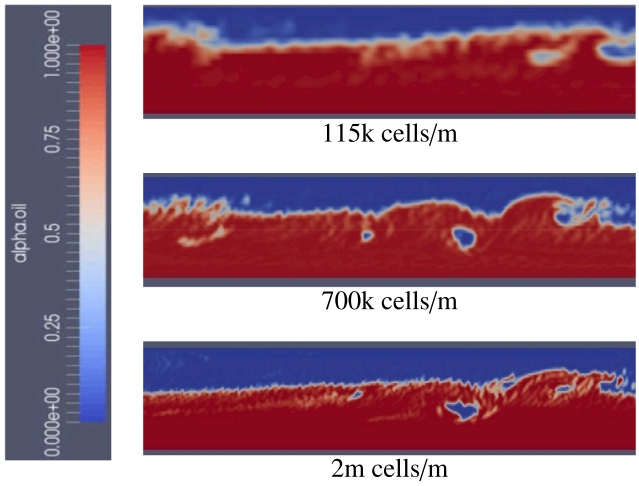

Fig. 21. Case #6, effect of mesh density on phase-mixing and bubble formation.

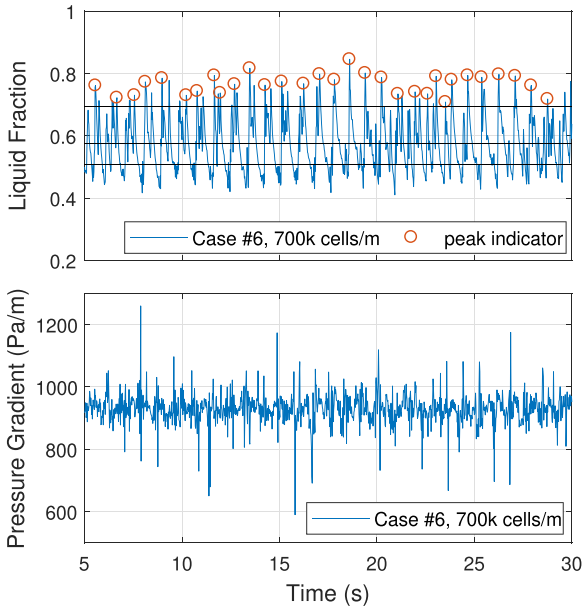

Fig. 22. Simulated liquid holdup fraction and pressure gradient as a function of time for 4° eccentric annulus case # 6 with 700 k cells/m and $E = 0.983$.

due to effect of the static head and higher mixture velocities, The simulated cases are within 35% of the experimental mean pressure gradient, and cases 6–8 are all within 10% of the mean. The threshold values are also better representation of the experiments. By increasing the mesh density for case #6 to 700 k (Fig. 22 and 2 million cells/m (Fig. 23) we noticed an increase in phase mixing (Fig. 21); however, there are no conventional slugs. see Fig. 30.

Fig. 21 shows that the number of light patches within the liquid (red) increases with mesh density, the increased gas entrapment is especially noticeable between 115 and 700 k cells/m. Unfortunately, even the 2 million cells/m mesh does not produce slug flow. Perhaps for a plug flow, which has less gas entrapment the mesh densities would be

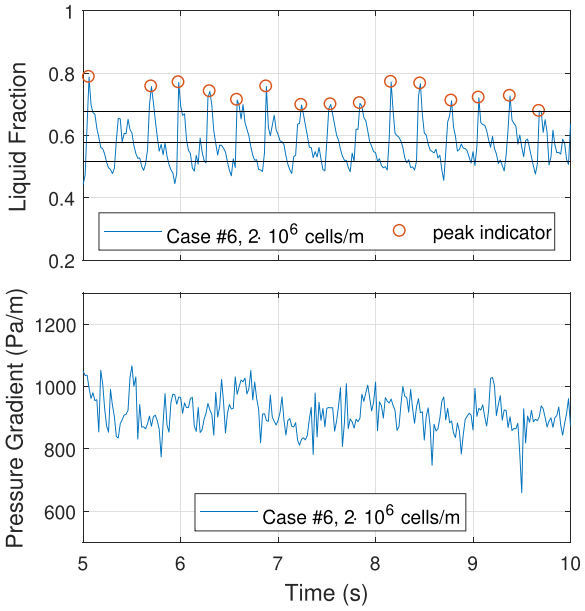

Fig. 23. Simulated liquid holdup fraction and pressure gradient as a function of time for 4° eccentric annulus case # 6 with 2 million cells/m and $E = 0.983$.

sufficient, which could be the reason why there are simulations of successful water–air slug flow, such as (Shuard et al., 2016). The higher surface tension between water and air results in less gas entrapment and spray from waves. It is also possible that phenomenological modeling of bubble formation, adaptive meshing or different turbulence models and boundary conditions would improve simulation accuracy.

Because the 2 million cells/m simulation requires such significant computational resources it was simulated for 10 s in a shortened domain. By analyzing similarly short periods for complete simulations it is found that the average and threshold values are well established even at a low sample count of 250.

As shown by Table 18, the mean pressure gradient decreases with mesh density, while the distance between mean and extreme values increases. It is appealing to theorize that the effect is triggered by increased phase-mixing, and ability to resolve minor structures and wall effects. Note that the frequency of the proto-slug structures is artificially increased for the finest mesh due to the shortened domain, an effect noted in both (Frank, 2005; Friedemann et al., 2019).

8.3. Simulated pressure gradient and holdup fraction results for eccentic annulus ($E = 0.983$) at 90° inclination with sulphur hexafluoride (gas) and Exxsol D60/Marcol 82 mixture (liquid)

The vertical cases behave differently than the $0-4^0$ cases. Mainly, due to the direction of gravity. Instead of encouraging layered flows with typical waves and slugs, vertical flow at these holdup fractions typically includes walls covered by a liquid film and a high velocity core. The resultant is a very high frequency holdup oscillation (Table 19) accompanied with a high mean pressure gradient (Table 20). The flow regime is difficult to determine by the holdup plots and externally images due to the liquid film wetting the cylinder walls. Compared to the experiments, the holdup peak frequency of the simulations is in reasonable agreement except for case 11, where the frequency is 0.47 Hz

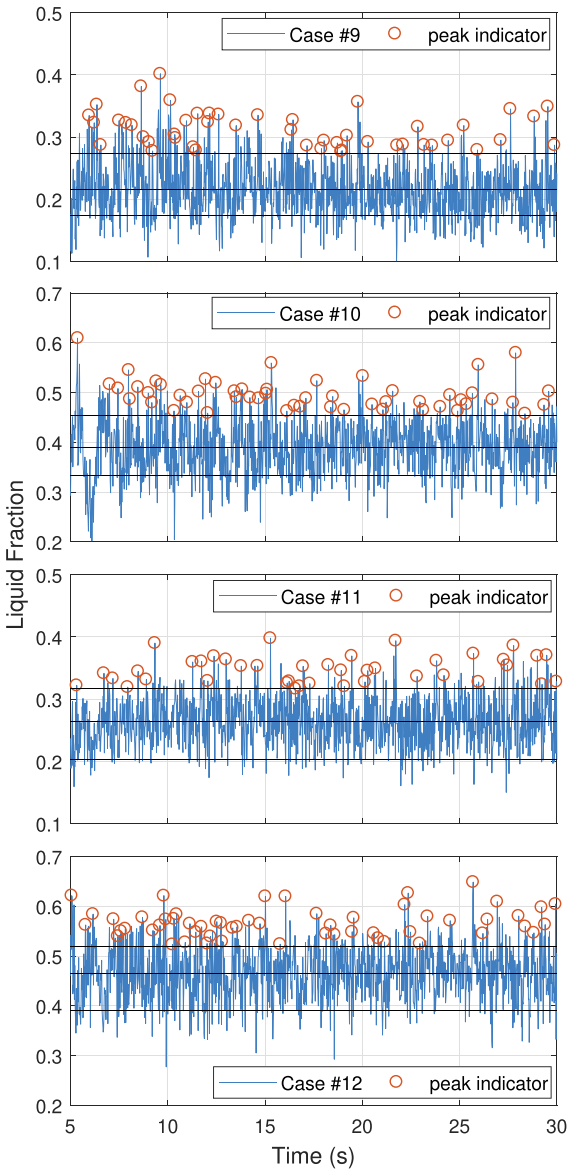

Fig. 24. Simulated liquid holdup fraction for 90° inclined eccentric annulus (E = 0.983) cases 9–12 with sulphur hexafluoride (gas) and Exxsol D60/Marcol 82 mixture (liquid).

higher than the experiment. For the remaining cases, the agreement is within 0.33 Hz.

From the experimental and computational (Figs. 25 & 26 imaging, a liquid film covering the outer cylinder and a gas core with flakes of liquid is visible, there is also a stream of gas passing through liquid near the contact line. The liquid film is periodically backflow, most prominently near the contact line between the two cylinders. The flow regime is most likely wispy annular or churn flow, possibly a transitional flow between the two flow regimes. The wispy annular flow regime was first identified by Bennett et al. (1965) and consists of a thin liquid film on the walls and long streaks or flakes of liquid within the gas core. The pressure gradient transients are referenced for further analysis.

The mean pressure gradients for the four vertical cases (Tables 20 & 21-22) are within 21% of and 36% of each threshold value. The pressure gradient can be sensitive to mesh density near the walls and contact line.

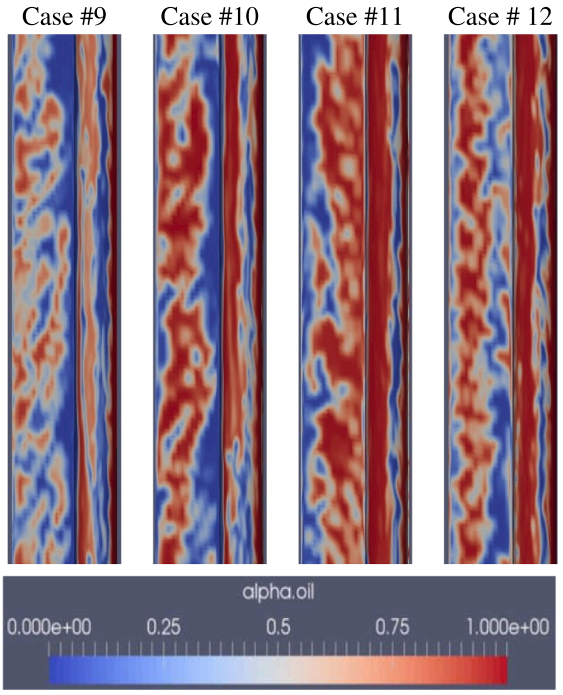

Fig. 25. Streamwise snapshots of simulated flow regime for vertical eccentric annulus cases.

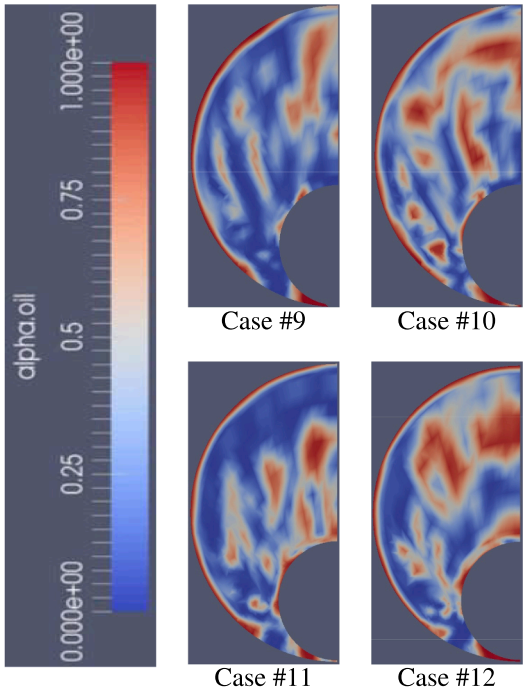

Fig. 26. Snapshots of cross-section of vertical eccentric annulus simulation cases.

In addition, any measurement error from the experiments related to, for example, the holdup fractions, will result in an error that follows through into the simulations as the initial conditions constrain the holdup fractions, and thereby affect the pressure gradient. Regardless, as

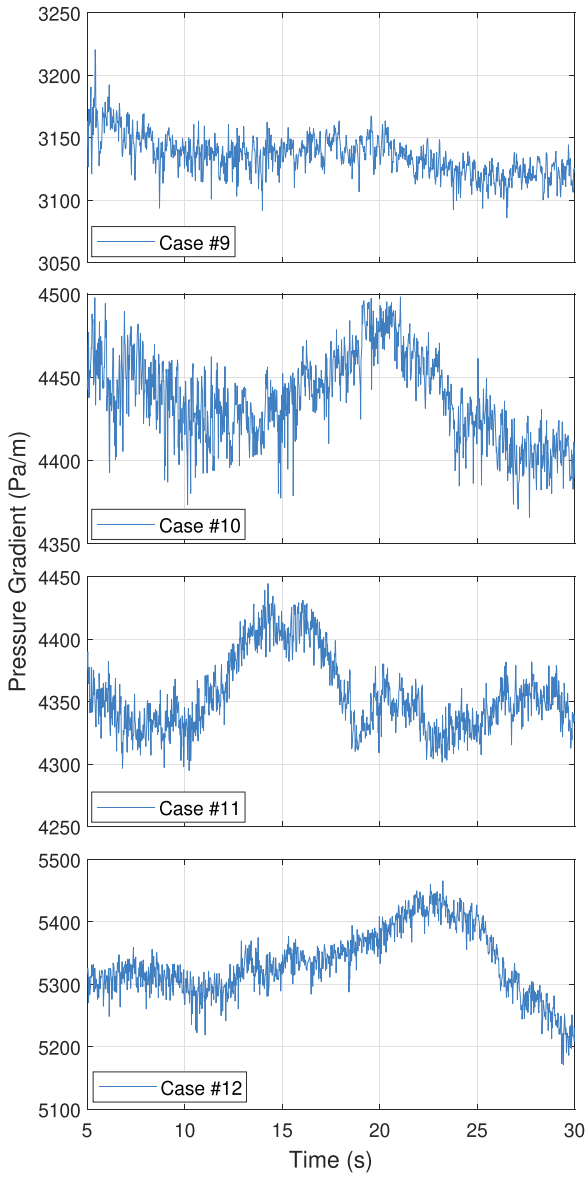

Fig. 27. Simulated pressure gradient as a function of time for 90° eccentric annulus (E = 0.983) cases 9–12 with sulphur hexafluoride (gas) and Exxsol D60/Marcol 82 mixture (liquid).

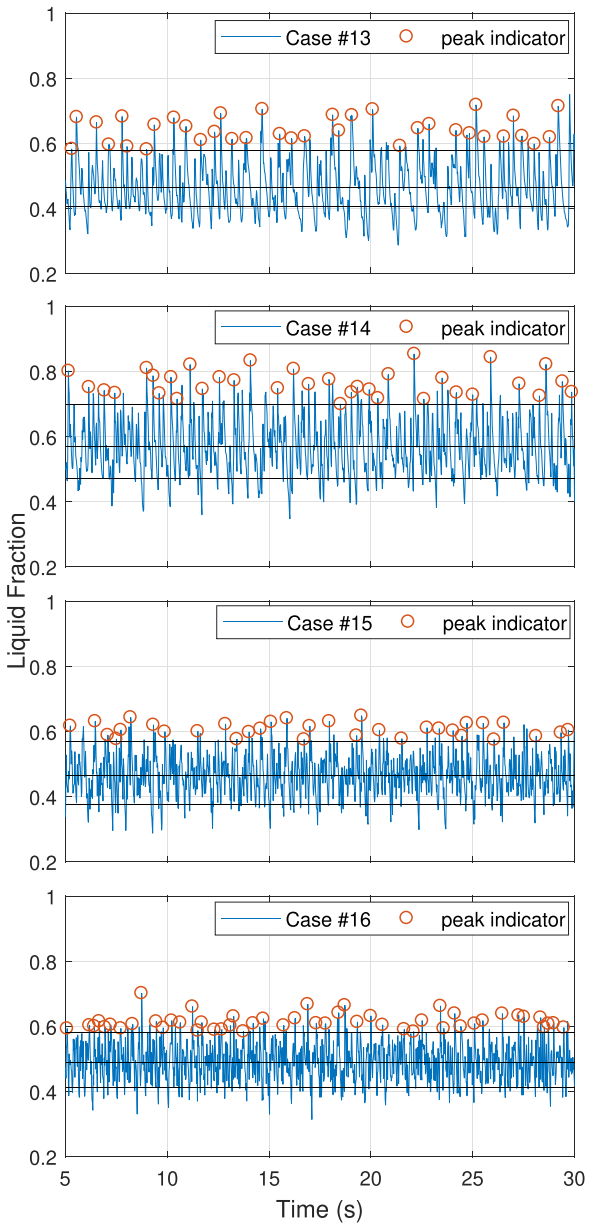

Fig. 28. Simulated liquid holdup fraction for 10° inclined eccentric annulus (E=.0983) cases 9–12 with sulphur hexafluoride (gas) and Exxsol D60/Marcol 82 mixture (liquid).

mentioned in Friedemann et al. (2019) interFoam in combination with a coarse mesh tends to over-predict the pressure gradient. see Table 23.

Concerning internal variations within the experiments themselves, by down-sampling to several distinct 25 s intervals, there are no noticeable changes in the experimental statistics. The simulations, on the other hand, for cases 10 and 11, appear to have two dominant frequencies (Fig. 27), with long-periodic oscillations of 100–150 Pa/m, which conforms to Hawkes et al. (2000) description of wispy annular flow. In order to confirm if there are multiple dominant frequencies, the time-series would have to be extended.

8.4. Simulated pressure gradient and holdup fraction results for eccentric annulus (E = 0.983) cases 13–16 at 10° inclination with sulphur hexafluoride (gas) and Exxsol D60/Marcol 82 mixture (liquid)

Cases 13–16 are the 10° versions of cases 5–9. The primary difference in flow development occurs for case # 13, which is reminiscent of a proto slug flow. The frequency of the proto slug is 1.4 Hz, which represents a significant increase of nearly 40% compared to the 4° case. The

Table 16
Summarized pressure gradient information for simulated 4° inclined fully eccentric annulus (E = 0.983).

Case #	5% (Pa/m)	mean (Pa/m)	95% (Pa/m)
5	641.9	661.5	681.7
6	941.2	965.3	989.7
7	1277.7	1299.7	1322.2
8	1609.5	1635.9	1661.7

Table 17
% Difference between simulated and experimental pressure gradient for 4° inclined eccentric annulus (E = 0.983) with sulphur hexaflouride (gas) and Exxsol D60/ Marcol 82 mixture (Liquid).

Case #	5% (%)	mean (%)	95% (%)
5	146	33.0	−15.1
6	45.8	−5.2	−28.0
7	50.2	9.4	−18.0
8	−0.42	−8.7	−15.1

Table 18
Summary of the pressure gradient and slug frequency for case # 6 at increasing mesh count and 4° inclination with E = 0.983

cells/m	5% (Pa/m)	mean (Pa/m)	95% (Pa/m)	f (Hz)
115 k	941.2	965.3	989.7	1.36
700 k	858.8	929.5	1000.4	1.24
2 m	830.7	916.5	1015.5	3.2
exp.	645.6	1018.7	1375.5	0.83

Table 19
Simulated holdup peak frequencies for 90° inclined eccentric (E = 0.983) with sulphur hexafluoride (gas) and Exxsol D60/Marcol 82 mixture (liquid).

Case #	frequency (Hz)
9	2.04
10	2.12
11	2.16
12	2.24

Table 20
Summary of simulated pressure gradient information for 90° eccentric annulus (E = 0.983) cases 9–12 with sulphur hexafluoride (gas) and Exxsol D60/Marcol 82 mixture (liquid).

Case #	5% (Pa/m)	mean (Pa/m)	95% (Pa/m)
9	3111.4	3135.6	3162.5
10	4395.0	4437.4	4480.5
11	4316.8	4355.0	4414.1
12	5248.7	5334.0	5426.6

Table 21
% Difference between simulated and experimental pressure gradient for vertical eccentric annulus cases 9–12.

Case #	5% (%)	mean (%)	95% (%)
9	36.4	28.5	22.3
10	14.3	9.4	6.3
11	28.6	20.7	14.4
12	0.96	1.1	1.5

Table 22
Simulated Wave and slug frequencies for eccentric annulus (E=.0983) cases 13–16 at 10° inclination with sulphur hexafluoride (gas) and Exxsol D60/Marcol 82 mixture (liquid).

Case #	Slug frequency (Hz)	Wave frequency (Hz)
13	–	1.40
14	1.40	–
15	1.32	–
16	2.0	–

Table 23
Summarized pressure gradient information for 10° inclined eccentric annulus simulation cases 13–16 (E = 0.983).

Case #	5% (Pa/m)	mean (Pa/m)	95% (Pa/m)
13	1020.6	1051.4	1078.7
14	1415.3	1453.7	1497.3
15	1678.7	1705.5	1730.8
16	2032.5	2061.9	2092.0

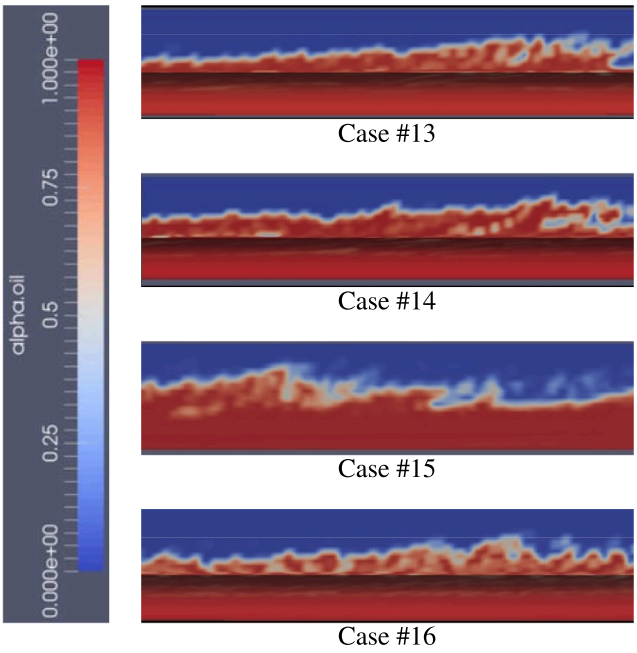

Fig. 29. Snapshots of simulated flow regime for 10° inclined eccentric annulus with E = 0.983.

added inclination results in steeper waves and higher peak holdup readings for all cases as well as higher peak frequency for most cases, although cases 14 and 15 show only minor frequency differences compared to the 4° cases.

The snapshots of the 10° inclined cases (Fig. 29) are consistent with the observations made for the 4° cases. However, there is an increased wave steepness and peak amplitude. There is also noticeably more spray ejected from the peaks of the waves and proto-slugs.

If the flow regimes across the 4° and 10^0 cases are consistent, there should be a pressure gradient increase dominated by hydrostatic forces. By increasing the inclination and enforcing a mixture velocity, the pressure gradient is increased in order to maintain the velocity. For sufficiently high inclination or sufficiently low Froude number, the gas velocity would most likely be significantly increased accompanied by a modest increase in the liquid velocity near the interface, while the lower liquid layer is stagnating or even moving backward.

The increase in mean pressure gradient from 4° to 10° is 389.9, 490.4, 405.8, and 426 Pa/m, respectively. The respective liquid holdup fractions are 0.45, 0.57, 0.46, and 0.49; by calculating the hydrostatic pressure component based on $P_{hydro} = \rho \cdot g \cdot L \cdot sin(\theta)$ and finding the pressure gradient by dividing by the domain length (L), then the expected change in mean pressure gradient due to hydrostatic pressure is 416.3, 515.5, 424.7 and 450.4 Pa/m. The difference between the actual increase and expected increase is within 18 to 27 Pa/m or 4 to 6.5%, this would be the change in the frictional pressure loss. Because these values are so close to the theoretical value, there is most likely only a minor effect of inclination on the flow regime in these cases.

9. Conclusions

In the present work, flow regime and pressure gradient behavior of

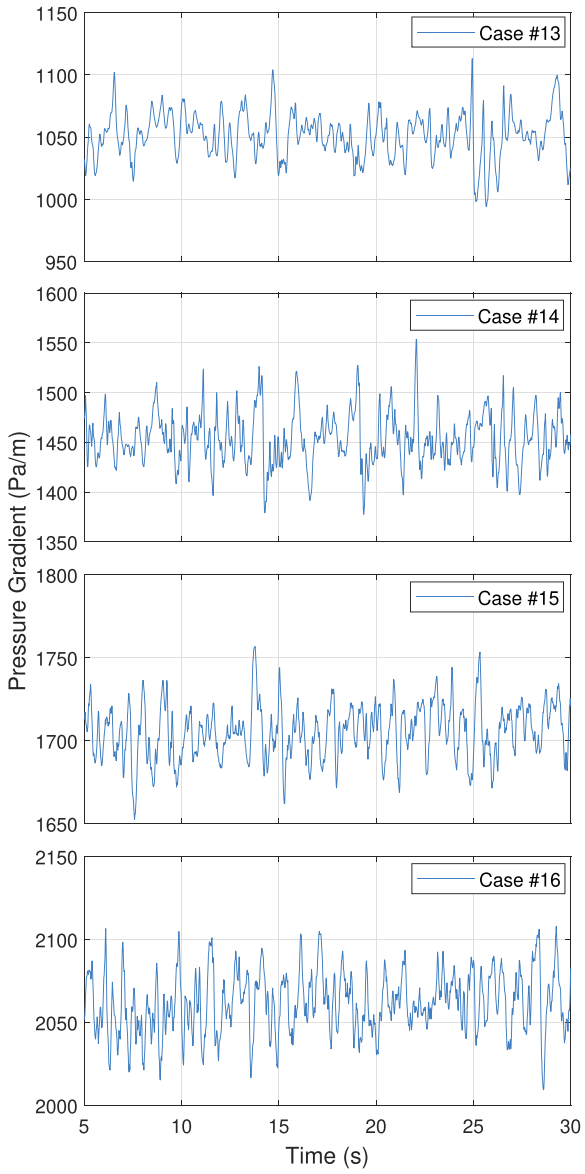

Fig. 30. Simulated pressure gradient as a function of time for eccentric annulus (E = 0.983) cases 13–16 at 10° inclination with sulphur hexafluoride (gas) and Exxsol D60/Marcol 82 mixture (liquid).

two-phase eccentric annulus simulations were analyzed and compared with experimental data at 0, 4, and 90° inclination, as well as flow prediction at 10° inclination.

- As found in previous work, conventional slugs are difficult to produce within this computational frame. There are several factors which can impede the development of slugs.
- The first possible contributing cause to the lack of the development of slugs, is the restricted fluid mixing and bubble permeation in the simulations. This issue can be overcome through excessively fine meshes, which can resolves minuscule gas bubbles entrapped within the liquid layer. We are aware that we can easily simulate slugs by artificially creating them through the initial conditions; however, that does not solve the issue of having them form naturally through physical interactions.
- Second, the surface tension affects the simulations, as several researchers have shown in hollow pipes when simulating water and gas. It is well known that the surface tension coefficient in such a flow is significantly higher than for the present studies, which lead us to believe that we could potentially force slugs by altering the surface tension. However, in doing so we would be deviating from attempting to replicate physical flows and instead creating imaginary compositions to a higher degree than the VOF mixture averaging procedure currently does. Other possible reasons for the lack of slug formation include, boundary conditions, the VOF model, and initial conditions.
- Running the simulations in a similar software program, such as Ansys Fluent, under the same conditions could help in understanding the root cause of the lack of conventional slugs.
- The horizontal cases (1–4) were previously studied within a partially eccentric domain (E = 0.5). Apart from case number 2, there was a reduced pressure gradient of 30–40% in the fully eccentric cases when compared to the simulations in the previous publication. This follows the established theory that the friction coefficient is reduced as eccentricity approaches 1 and is in line with existing literature that is available for single-phase flows.
- For the cases where the inclination was increased by 6 degrees (cases 13–16), there was only a small effect on the flow regime compared to cases 5–8.
- For the cases described above (5–8, 13–16), a pressure gradient increase within 6.5% of the theoretical increase due to hydrostatic pressure increase was detected. This 6.5% increase is due to the change in frictional pressure gradient and was found by subtracting out the hydrostatic component. We believe this indicates that the inclination change had little effect on the resultant flow regime of the 10° cases compared to the cases at 4°.
- Simulation cases 1–12 are compared to experiments of the same mixture velocity and phase fractions. For all cases except 1 and 2, the mean pressure gradient is within 33% of the expected behavior. While there is a larger discrepancy for the minimum pressure gradient, the maximum pressure gradient is within 30% for cases 3–12.
- The wave and slug frequencies for cases 1–12 are consistent with observed behavior of the experiments. All analyzed cases are within 0.5 Hz, which in some cases appears as a significant discrepancy. However, by down-sampling the experiments to 25 s, it is found that there are large variations of the wave and slug frequency in the experiments themselves, which include the sampled simulation frequency.
- Comparing the simulated and experimental flow regimes with predicted flow regimes using the Barnea unified model, and a Taitel flow regime map, the flow regime is correctly predicted for all but 3 experimental cases and 4 simulated cases.

Through the present study, the effect on the pressure gradient by increasing the eccentricity of the annulus is measured. In comparing these results to previously published work, it was found to be in line with existing literature and the simulations are in reasonable agreement with the experimental data, even at low mesh densities. Lastly the effect of a minor increase in inclination was determined to have only a small effect on the flow regime, and the increased pressure gradient due to inclination was nearly an exact match to the theoretical increase.

Declaration of Competing Interest

The authors declare that they have no known competing financial interests or personal relationships that could have appeared to influence the work reported in this paper.

Acknowledgements

This work is part of a larger project called Multiphase Flow in Concentric and Eccentric Annulus Spaces (project number 255481) and has been performed thanks to funding from the Research Council of Norway through the PETROMAKS2 programme.

References

Adachi, T., Imai, S., 2007. Three-dimensional linear stability of natural convection in horizontal concentric annuli. Int. J. Heat Mass Transf. 50, 1388–1396. https://doi.org/10.1016/j.ijheatmasstransfer.2006.09.029.

Axtmann, G., Rist, U., 2016. Scalability of OpenFOAM with Large Eddy Simulations and DNS on High-Performance Systems. https://doi.org/10.13140/RG.2.1.2395.8000.

Barnea, D., 1987. A unified model for predicting flow-pattern transitions for the whole range of pipe inclinations. Int. J. Multiph. Flow 13 (1), 1–12. https://doi.org/10.1016/0301-9322(87)90002-4.

Bennett, B.A.W., Hewitt, G.F., Kearsey, H.A., Keeys, R.K.F., Lacey, P.M.C., 1965. Paper 5: Flow visualization studies of boiling at high pressure. Proceedings of the Institution of Mechanical Engineers, Conference Proceedings 180 (3), 260–283. https://doi.org/10.1243/PIME_CONF_1965_180_119_02.

Berberovic, E., 2010. Investigation of Free-surface Flow Associated with Drop Impact: Numerical Simulations and Theoretical Modeling (Ph.D. thesis). Technische Universität; Darmstadt. URL: http://tuprints.ulb.tu-darmstadt.de/2319/.

Berberovic, E., Hinsberg, N.V., Jakirlic, S., Roisman, I., Tropea, C., 2009. Drop impact onto a liquid layer of finite thickness: Dynamics of the cavity evolution. Phys. Rev. E, Stat., Nonlinear, Soft Matter Phys. 79, 036306 https://doi.org/10.1103/PhysRevE.79.036306.

Caetano, E., 1985. Upward Vertical Two-Phase Flow Through an Annulus (Ph.D. thesis), The University of Tulsa.

Das, G., Das, P., Purohit, N., Mitra, A., 1998. Rise velocity of a taylor bubble through concentric annulus. Chem. Eng. Sci. 53 (5), 977–993. https://doi.org/10.1016/S0009-2509(97)00210-8.

Denton, J., 1963. Turbulent Flow in Concentric and Eccentric Annuli. Master's thesis;. The University of British Columbia. https://doi.org/10.14288/1.0105462.

Erge, O., Vajargah, A.K., Ozbayoglu, M.E., van Oort, E., 2015. Frictional pressure loss of drilling fluids in a fully eccentric annulus. J. Natural Gas Sci. Eng. 26, 1119–1129. https://doi.org/10.1016/j.jngse.2015.07.030.

Ferroudji, H., Hadjadj, A., Haddad, A., Ofei, T.N., 2019. Numerical study of parameters affecting pressure drop of power-law fluid in horizontal annulus for laminar and turbulent flows. J. Petrol. Explor. Prod. Technol. 9 (4), 3091–3101. https://doi.org/10.1007/s13202-019-0706-x.

Frank, T., 2005. Numerical simulation of slug flow regime for an air-water two-phase flow in horizontal pipes. In: The 11th International Topical Meeting on Nuclear Reactor Thermal-Hydraulics. Avignon, France.

Friedemann, C., Mortensen, M., Nossen, J., 2019. Gas-liquid slug flow in a horizontal concentric annulus, a comparison of numerical simulations and experimental data. Int. J. Heat Fluid Flow 78. https://doi.org/10.1016/j.ijheatfluidflow.2019.108437.

Friedemann, C., Mortensen, M., Nossen, J., 2020. Two-phase flow simulations at 0-4° inclination in an eccentric annulus. Int. J. Heat Fluid Flow 83.https://doi.org/10.1016/j.ijheatfluidflow.2020.108586.

Gomez, L.E., Shoham, O., Schmidt, Z.C., N.R., Brown, A., Northug, T., 1999. A unified mechanistic model for steady-state two-phase flow in wellbores and pipelines. Soc. Petrol. Eng.https://doi.org/10.2118/56520-MS.

Hamad, F., Khan, M., 1998. Natural convection heat transfer in horizontal and inclined annuli of different diameter ratios. Energy Convers. Manage. 39 (8), 797–807. https://doi.org/10.1016/S0196-8904(97)10010-3.

Hanks, R.W., Bonner, W.F., 1971. Transitional flow phenomena in concentric annuli. Ind. Eng. Chem. Fundamentals 10 (1), 105–113. https://doi.org/10.1021/i160037a018.

Harvel, G., Hori, K., Kawanishi, K., Chang, J., 1999. Cross-sectional void fraction distribution measurements in a vertical annulus two-phase flow by high speed x-ray computed tomography and real-time neutron radiography techniques. Flow Meas. Instrum. 10 (4), 259–266. https://doi.org/10.1016/S0955-5986(99)00008-4.

Hawkes, N., Lawrence, C., Hewitt, G., 2000. Studies of wispy-annular flow using transient pressure gradient and optical measurements. Int. J. Multiph. Flow 26, 1565–1582. https://doi.org/10.1016/S0301-9322(99)00104-4.

Hernandez-Perez, V., 2008. Gas-liquid two-phase flow in inclined pipes (Ph.D. thesis).

Hills, J., Chéty, P., 1998. The rising velocity of taylor bubbles in an annulus. Chem. Eng. Res. Des. 76 (6), 723–727. https://doi.org/10.1205/026387698525423.

Ibarra, R., Nossen, J., 2019. Investigation of oil-water flow in concentric and fully eccentric annuli pipes. Chem. Eng. Sci.: X 4. https://doi.org/10.1016/j.cesx.2019.100042, 100042, URL: http://www.sciencedirect.com/science/article/pii/S2590140019300498.

Iyer, S., Vafai, K., 1998. Buoyancy induced flow and heat transfer in a cylindrical annulus with multiple perturbations. Int. J. Heat Mass Transf. 41 (20), 3025–3035. https://doi.org/10.1016/S0017-9310(98)00053-2.

Julia, J.E., Hibiki, T., 2011. Flow regime transition criteria for two-phase flow in a vertical annulus. Int. J. Heat Fluid Flow 32 (5), 993–1004. https://doi.org/10.1016/j.ijheatfluidflow.2011.06.001.

Kalitzin, G., Medic, G., Iaccarino, G., Durbin, P., 2005. Near-wall behavior of rans turbulence models and implications for wall functions. J. Comput. Phys. 204 (1), 265–291. https://doi.org/10.1016/j.jcp.2004.10.018. URL: http://www.sciencedirect.com/science/article/pii/S0021999104004164.

Kelessidis, V., Dukler, A., 1989. Modeling flow pattern transitions for upward gas-liquid flow in vertical concentric and eccentric annuli. Int. J. Multiph. Flow 15 (2), 173–191. https://doi.org/10.1016/0301-9322(89)90069-4.

Kelessidis, V., Dukler, A., 1990. Motion of large gas bubbles through liquids in vertical concentric and eccentric annuli. Int. J. Multiph. Flow 16 (3), 375–390. https://doi.org/10.1016/0301-9322(90)90070-Y.

Kiran, R., Ahmed, R., Salehi, S., 2020. Experiments and cfd modelling for two phase flow in a vertical annulus. Chem. Eng. Res. Des. 153, 201–211. https://doi.org/10.1016/j.cherd.2019.10.012.

Liu, F., 2016. A thorough description of how wall functions are implemented in openfoam. In: Nilsson, H., (Ed.) Proceedings of CFD with OpenSource Software. URL: http://www.tfd.chalmers.se/hani/kurser/OS_CFD_2016.

Mizushima, J., Hayashi, S., Adachi, T., 2001. Transitions of natural convection in a horizontal annulus. Int. J. Heat Mass Transf. 44, 1249–1257. https://doi.org/10.1016/S0017-9310(00)00188-5.

Nikitin, N., Wang, H., Chernysenko, S., 2009. Turbulent flow and heat transfer in eccentric annulus. J. Fluid Mech. 638:95–116.https://doi.org/10.1017/S002211200900812X.

Nuland, S., 1999. Bubble fraction in slugs in two-phase flow with high viscosity liquid. In: Proceedings of the 2nd International Symposium on Two-phase Flow Modeling and Experimentation. Pisa, Italy. https://doi.org/10.1088/1757-899X/121/1/012018.

Ozar, B., Jeong, J., Dixit, A., Juliá, J., Hibiki, T., Ishii, M., 2008. Flow structure of gas-liquid two-phase flow in an annulus. Chem. Eng. Sci. 63, 3998–4011. https://doi.org/10.1016/j.ces.2008.04.042.

Ozbayoglu, A.M., Yuksel, H.E., 2012. Analysis of gas-liquid behavior in eccentric horizontal annuli with image processing and artificial intelligence techniques. J. Petrol. Sci. Eng. 81, 31–40. https://doi.org/10.1016/j.petrol.2011.12.008.

Ozbayoglu, E., Sorgun, M., 2010. Frictional pressure loss estimation of non-newtonian fluids in realistic annulus with pipe rotation. J. Can. Petrol. Technol. 49, 57–64. https://doi.org/10.2118/141518-PA.

Rusche, H., 2002. Computational fluid dynamics of dispersed two-phase flows at high phase fractions (Ph.D. thesis). Imperial College London; Exhibition Road, London SW7 2BX. URL: https://spiral.imperial.ac.uk/handle/10044/1/8110.

Shoham, O., 2006. Mechanistic modeling of gas-liquid two-phase flow in pipes. Soc. Petrol. Eng.

Shuard, A., Ben, Mahmud H., King, A., 2016. Comparison of two-phase pipe flow in openfoam with a mechanistic model. IOP Conf. Ser.: Mater. Sci. Eng. 121, 012018 https://doi.org/10.1088/1757-899X/121/1/012018.

Taitel, Y., Barnea, D., Dukler, A.E., 1980. Modelling flow pattern transitions for steady upward gas-liquid flow in vertical tubes. AIChE J. 26 (3), 345–354. https://doi.org/10.1002/aic.690260304.

Taitel, Y., Dukler, A., 1976. A model for predicting flow regime transitions in horizontal and near horizontal gas-liquid flow. AIChe J. 22, 47–55. https://doi.org/10.1002/aic.690220105.

Vaughn, R., 1963. Laminar flow of non-newtonian fluids in concentric annuli. Soc. Petrol. Eng. 3, 274–276. https://doi.org/10.2118/615-PA.

Wongwises, S., Pipathattakul, M., 2006. Flow pattern, pressure drop and void fraction of two-phase gas-liquid flow in an inclined narrow annular channel. Exp. Thermal Fluid Sci. 30, 345–354. https://doi.org/10.1016/j.expthermflusci.2005.08.002.

Yoo, J., 2003. Dual free-convective flows in a horizontal annulus with a constant heat flux wall. Int. J. Heat Mass Transf. 46, 2499–2503. https://doi.org/10.1016/S0017-9310(02)00539-2.

Yu, B., Kawaguchi, Y., Kaneda, M., Ozoe, H., Churchill, S., 2005. The computed characteristics of turbulent flow and convection in concentric circular annuli. part ii. uniform heating on the inner surface. Int. J. Heat Mass Transf. 48, 621–634. https://doi.org/10.1016/j.ijheatmasstransfer.2004.08.022.